January 2023

Buckling Behavior Of Metallic Thin-Walled Stiffened Cylindrical Shells Under Static Loading

Fnu Tabish

Buckling Behavior of Metallic Thin-Walled Stiffened Cylindrical Shells Under Static Loading

by

FNU Tabish

A Thesis

Submitted to the Graduate Faculty

of the

University of North Dakota

in partial fulfillment of the requirements

for the degree of

Master of Science

Civil Engineering

College of Engineering and Mines

Grand Forks, North Dakota

August

2023

This thesis, submitted by FNU Tabish in partial fulfillment of the requirements for the Degree of Master of Science in Civil Engineering from the University of North Dakota, has been read by the Faculty Advisory Committee under whom the work has been done and is hereby approved.

6/24/2023

Dr. Iraj H.P. Mamaghani (Chairperson)

6/23/2023

Dr. Nabil Suleiman

7/18/2023

Dr. Cai Xia Yang

This thesis is being submitted by the appointed advisory committee as having met all of the requirements of the School of Graduate Studies at the University of North Dakota and is hereby approved.

Dr. Chris Nelson, Associate Dean

School of Graduate Studies

Date

PERMISSION

Title: Buckling Behavior of Metallic Thin-Walled Stiffened Cylindrical Shells Under Static Loading

Department: Civil Engineering

Degree: Master of Science (MSc.)

In presenting this thesis in partial fulfillment of the requirements for a graduate degree from the University of North Dakota, I agree that the library of this University shall make it freely available for inspection. I further agree that permission for extensive copying for scholarly purposes may be granted by the professor who supervised my thesis work or, in his absence, by the Chairperson of the department or the dean of the Graduate School. It is understood that any copying or publication or other use of this thesis or part thereof for financial gain shall not be allowed without my written permission. It is also understood that due recognition shall be given to me and to the University of North Dakota in any scholarly use which may be made of any material in my thesis.

FNU Tabish

August 2023

TABLE OF CONTENTS

LIST OF FIGURES

LIST OF TABLES

ACKNOWLEDGEMENTS

I wish to express my sincere appreciation and gratitude to Dr. Iraj H.P. Mamaghani, my advisor, for his guidance and support during my time in the master's program at the University of North Dakota. My sincere thanks also extended to my committee members, Dr. Nabil Suleiman and Dr. Cai Xia Yang for their valuable support and advice to complete this thesis.

LIST OF PUBLICATIONS

Peer Reviewed Journal Papers

1) **Tabish**, Raza Ali, Shafiullah, Jameel M.S., (2022). Investigation of flexural behavior of reinforced concrete beams using 3D finite element analysis. *Numerical Methods in Civil Engineering*, 7-1, 37-56.

2) **Tabish FNU,** Mamaghani H.P. I., (2023). Buckling Behaviour of Thin-Walled Stiffened-Aluminium Cylindrical Shells Subjected to External Lateral Pressure. *Thin-Walled Structures* (Paper Submitted)

Peer Reviewed Conferences

1) **Tabish FNU**, Mamaghani, I.H.P. (2022). Buckling Analysis of Cylindrical Steel Fuel Storage Tanks under Static Forces, The *7th International Conference on Civil Structural and Transportation Engineering (ICCSTE'22) virtual conference*, June 05-07, 2022, Paper ID 243.

2) **Tabish FNU**, Mamaghani, I.H.P. (2023). Buckling Behavior of Ring Stiffened-Aluminium Cylinders Subjected to External Pressure, *Proceedings of International Structural Engineering and Construction, ISSN 2644-108X, Vol. 10(1), ISEC Press, August 2023* (Manuscript Accepted).

3) **Tabish FNU**, Mamaghani, I.H.P. (2023). Numerical Buckling Behavior of Perfect and Imperfect Steel Cylinders Under External Pressure, *Proceedings of International Structural Engineering and Construction, ISSN 2644-108X, Vol. 10(1), ISEC Press, August 2023* (Manuscript Accepted).

4) Morris C., Schneider D., Mwaura N., **Tabish FNU**, Carpenter D.,Clark N., Sandip A., (2023). Graphics Processing Units' Accelerated Navier-Stokes Solvers for Unstructured Meshes: A Literature Review, *Proceedings of the ASME 2023 International Mechanical Engineering Congress and Exposition, IMECE 2023* (Manuscript Submitted).

ABSTRACT

This thesis aims to estimate and improve the buckling strength of the cylindrical storage tanks under static loadings. Initially, for the verification of the overall performance of the numerical modeling approach; a computational analysis was conducted to calculate the linear buckling behaviour of empty cylindrical shells with different *H/D* and *D/t* ratios using ANSYS workbench 2021. Results revealed that the FE models accurately predict static critical buckling stress which is mainly depends on the *D/t* ratio. The solution of the buckling analysis provides multiple buckling mode shapes and critically buckling load values. Those mode shapes (eigenvectors) can indicate the expected buckling modes during the nonlinear analysis.

For steel made cylindrical specimens subjected to external pressure; varying *R/t* and *H/R* ratios strongly influence the critical buckling pressure. The buckling pressure remarkably increases with the decrease of both *R/t* and *H/R* ratios; however, the effect of the *R/t* ratio is more dominant than the *H/R* ratio. The Results revealed that the geometric imperfections have little influence on the overall buckling capacity, especially for tanks with large *H/R* ratios and smaller *R/t* ratios. Numerical results show good agreement with experimental and theoretical results; however, FEA gave higher results, especially for cylinders with smaller *R/t* ratios might be due to neglecting imperfections that are probably created in the construction process.

For Aluminium made thin-walled ring stiffened cylindrical specimens subjected to the external pressure; A comprehensive finite element (FE) numerical study investigated the influence of external ring stiffeners varying from 3 to 17 on a thin-walled, stiffened aluminium cylindrical shell buckling strength. Ten ring-stiffened cylindrical specimens were modeled using an ANSYS workbench 2021 whose stiffener dimensions varied so that all specimens' overall weight remained constant. FE linear and nonlinear buckling results were compared with the experimental work and the theoretical formulas in the literature. The failure mode shapes and number of circumferential lobes at failure for all specimens obtained from the linear analysis closely matched the experimental failure pattern. The linear buckling pressures were lower than the corresponding experimental critical pressures; however, they compare well with the buckling pressure obtained from the theoretical equations. The nonlinear buckling pressures for perfect geometries are lesser than the experimental pressures, and specimens with nine or fewer stiffeners were crushed instead of buckling at failure. For nonlinear analysis of imperfect geometries based on the eigenmode shape, results revealed that the 5 % imperfection giving the failure mode shapes similar to the experimental buckling shapes for most of the specimens, and local shell buckling pressures were closer to the experimental buckling pressures compared to the overall flexural buckling results. The overall FE results indicate that the failure mode types shifted from shell local buckling mode to the flexural buckling mode while increasing the number of ring stiffeners by keeping the specimen's overall weight constant. Parametric study reveals that linear and nonlinear buckling strength remarkably improved by keeping a constant stiffener height compared to the FE buckling strength for specimen dimensions obtained from experiments, especially for specimens that failed with overall flexural buckling mode. The experimental, theoretical, and finite element (FE) results proved that the ring stiffener's optimum size and spacing could improve the stiffened cylinder buckling strength since critical buckling pressure and failure mode shape were influenced by the ring stiffener's size and spacing.

1 Introduction

1.1 Thin Wall Cylindrical Storage Tanks

Nowadays, thin-walled cylindrical shell structures are remarkably used as storage vessels because of their economic and efficient support system. Due to the very slim and thin-walled cylindrical nature, the buckling response of the cylindrical tanks results in a sudden and significant change in the structural configuration [1]. This unstable buckling response of cylindrical tanks results, a large deflection and a substantial reduction in load bearing capacity and stiffness of the tanks. Furthermore, stability issue arises due to the initial geometric imperfection that is the small unintended variations in the geometry results from the manufacturing process [2]. When a liquid storage tank is subjected to the natural forces it can be failure and damaged ultimately causing the leakage of toxic liquid inside which become a serious threat to human health and the environment [3]. Additionally, the failure of inflammable substance containing tanks has frequently led to the major fires. Some common failure types of cylindrical shell structures are illustrated in Figure 1-1. Therefore, the prevention of the buckling and large magnitude displacement against static and dynamic forces is the primary design problems which requires fully attention.

(a) (b) (c) (d)

Figure 1-1. Failure types: (a) Elephant foot buckling, (b) Diamond shape buckling, (c) Connection failure, (d) Buckling due to negative internal pressure.

It should be cited that the stiffened thin-walled shell structures (built as a combination of thin plates and strong stiffeners, such as rings and stringers) is one of the effective solutions to enhance the material efficiency and structural sustainability [4]. Thin-walled plates with stiffeners will provide a sufficient resistance against buckling due to compressive and seismic forces. The load-increasing effect of stiffened thin-walled shell structure under these forces has received a limited attention until today. Not neglecting this combination will lead to more economical and safer construction. Therefore, casting light on this seldom considered new development will improve the design approaches for such structures.

1.2 Research Objectives

The primary goal of this study is to evaluate the buckling behavior of thin wall stiffened cylindrical shells under the influence of static loading. To accomplish this goal, comprehensive analytical research is conducted with the following main objectives.

The main objectives of this research are:

- To obtain the failure buckling loads of stiffened and unstiffened thin wall cylinders under the influence of static loadings.
- Assessment of the effect/influence of imperfections and boundary conditions on the buckling behavior of thin-walled stiffened cylinders.
- Find out the possible modes of failure based on a simple tool under the application of static loading.
- To study the effect of following parameters on the buckling load of the stiffened cylinders: radius-to-thickness ratio, length-to-radius ratio, geometry of the stiffeners and distance of stiffeners.

1.3 Organization of the Thesis

This thesis consists of six chapters, as illustrated in Figure 1-2. The current chapter provides a comprehensive introduction about thin well cylindrical storage tanks and their stability issues under the influence of natural forces, as well as the necessity for conducting new parametric studies. Chapter 2 deals with the brief history related to the experimental and numerical works conducted to gain insights into the behavior of stiffened and unstiffened thin-walled cylindrical tanks subjected to static loads. Chapter 3 deals with the verification of FE modelling. A linear analysis was performed to calculate the linear buckling behaviour of empty cylindrical shells with different *H/D* and *D/t* ratios using commercial engineering software ANSYS workbench 2021. The theoretical results were compared with FE analysis results to substantiate the model.

Chapter 4 deals with the numerical buckling behavior of perfect and imperfect unstiffened steel cylinders with varying *R/t* and *H/R* ratios under external pressure. Twelve specimens were analysed with both linear and nonlinear analysis. Real imperfections were considered to investigate the buckling behavior of imperfect geometries and results are substantiated with the experimental results obtained from the literature. In chapter 5, a comprehensive numerical study was conducted to investigate the influence of external ring stiffeners varying from 3 to 17 on a thin walled, stiffened aluminium cylindrical shell buckling strength. Linear analysis, nonlinear analysis with perfect geometries, and nonlinear analysis with imperfect geometries based on eigen modes shapes were considered to investigate the buckling behavior of ten ring-stiffened cylindrical specimens whose stiffener dimensions varied so that all specimens' overall weight remained constant. Finite element results are substantiated with theoretical and experimental results. Further parametric studies are added to improve the buckling strength. Finally, the conclusions and future work are summarized in Chapter 6.

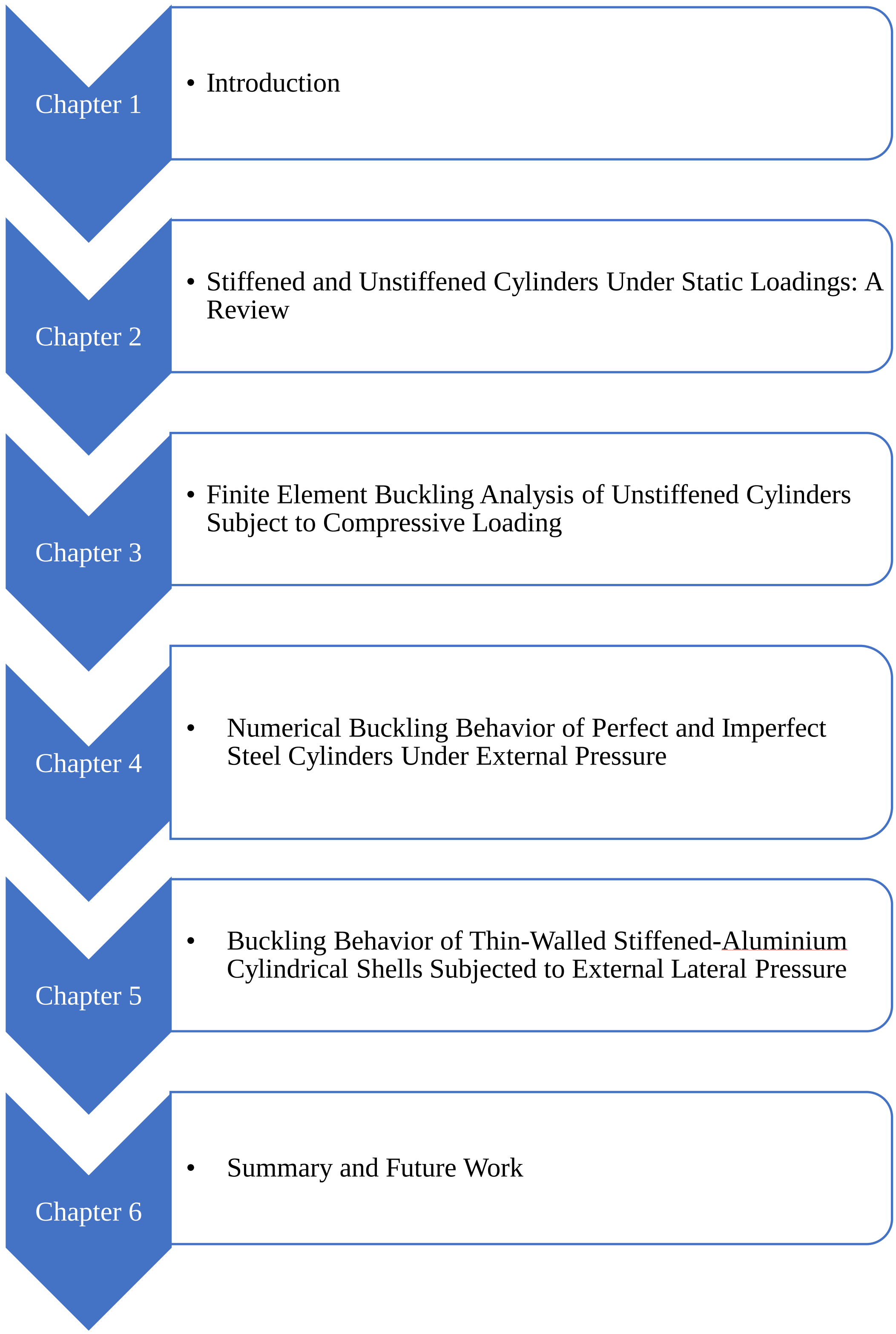

Figure 1-2. Organization of the chapters

2 Stiffened and Unstiffened Cylinders Under Static Loadings: A Review

This chapter consists of a brief introduction and background limited to the experimental and numerical works on stiffened and unstiffened cylindrical tanks. This portion of the report has been submitted to a peer-reviewed journal for publication and will be accessible publicly upon acceptance.

2.1 Introduction

Shell buckling is the most common failure phenomenon for thin-walled cylindrical shell structures due to their very slim and thin nature. The critical buckling load of the shell primarily depends on geometrical configuration, material properties, the way it is stiffened, loading, and boundary conditions [2]. Stiffened thin-walled shell structures built as a combination of thin plates and strong stiffeners, such as rings and stringers, are often used to enhance buckling resistance and structural stability. Ring stiffeners are preferable to stringers to enhance the thin-walled shell buckling resistance while subjected to external lateral pressure [4].

Ring-stiffened shells under external lateral pressure may fail in one or more of the three modes: shell local buckling, flexural buckling, and axisymmetric failure, illustrated in Figure 2-1[4]. The stiffened cylinders with strong ring stiffeners failed either with shell local buckling or axisymmetric local buckling in nature, and stiffened cylinders with lighter ring stiffeners failed with overall flexural buckling mode; therefore, ring stiffeners are primarily used to enhance the local shell buckling strength.

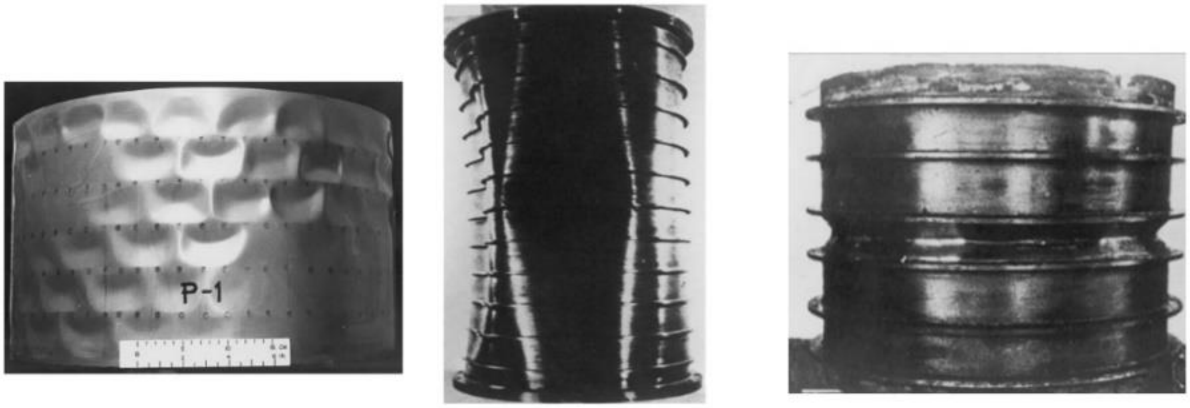

(a) (b) (c)

Figure 2-1. Buckling modes for ring-stiffened cylinders subjected to external lateral pressure (a) Local shell buckling (b) Overall flexural buckling (c) Local axisymmetric buckling

2.2 Background

Three main approaches are involved in analyzing stiffened shell structures: theoretical analysis, experimental investigation, and numerical simulation. A brief history limited to the experimental and numerical works on stiffened cylindrical tanks is presented here. The stiffened shell buckling analysis is usually based on the energy method due to its complex behavior. A simply supported, stiffened cylindrical shell buckling analysis while subjected to hydrostatic pressure was first conducted by Kendrick [5] and Nash [6]. Then in succeeding years, their theoretical predictions were experimentally verified by Galletly *et al.* [7]. Besides Kendrick's solution, the most widely used design equation is that of Bryant [8]. Kendrick's equation has been recommended by BS 5500 1997 [9], while Bryant's formula has been adopted by American Structural Steel Research Council (SSRC) [10]. Early experimental studies revealed that the stiffened cylinder buckling strength mainly depends on the stiffener's properties. According to Weller and Singer, [11] stiffened cylinder exhibits a higher buckling load than the unstiffened cylinder with equivalent mass. This increased buckling strength depends on stiffener properties such as cross-section, spacing, eccentricity, direction, or pattern. The authors performed experiments on 158 stringer-stiffened shells and proved the stiffened shell structural efficiency on the equivalent weight isotropic shells. Miller [12] reported tests on 41 small-scale specimens with and without stiffeners. The author also performed four large-scale experiments on storage tanks with stiffeners made from three different steel grades and six sheets having a radius-to-thickness ratio (R/t) ranging from 250 to 750. The author observed that elastic buckling capacity mainly depends on the radius to thickness ratio (R/t) ratio. Buckling strength increased using stiffeners, and longer cylindrical experimental data exhibited more scattered results than the shorter stiffened cylinders.

Early research on stiffened cylinders was based on their application in the aerospace industry. An extensive technological transformation from the aerospace industry to the offshore structure occurred after 1970. British Department of Energy and Science Research Council conducted extensive experimental research on small and large stiffened shells for marine structures at four different UK universities in the early 1980s [13], [14], [15]. This research work provided a significant offshore steel shell analysis and design database. Seliem and Roorda [16] conducted experimental work on ten aluminium-made stiffened shells with ring stiffeners varying from 3 to 17 to investigate the ring stiffener's effect on buckling mode and critical pressure under the influence of external pressure. The stiffener's size, number, and spacing were varied so that the overall weight remained constant. Failure pressure, strain, and buckling deformations were measured using an experimental setup. The critical buckling pressure from experimental buckling modes was calculated by using the Southwell method. Tian *et al.* [17] proposed a new eigenvalue solution via the Ritz method to investigate the overall ring-stiffened cylindrical shell buckling pressure under the influence of general lateral pressure, with varying boundary conditions and different longitudinal ring stiffeners distribution. The final equation possessed some unique features to handle various ring stiffener shapes, any combination of boundary conditions, and varying lateral pressure.

Kransovsky and Kostyrko [18] used vertical stiffeners in two different series based on length, such as series No. 1 had 24 stringers and sequence No. 2 had 36 stringers. The authors also considered two boundary conditions: simply supported and fully clamped for all specimens. The specimens were manufactured from cold rolled stainless steel with inner and outer stringers, a radius to thickness ratio (*R/t*) equal to 376, and a height-to-radius ratio (*L/R*) varying from 0.28 to 2.80. Only simply supported shells with series No. 2 inner stiffeners indicate a good correlation between experimental and theoretical results. Cerik et al. [19], Cerik and Cho [20], and Cheo at al. [21] partially reported few test models on welded ring stiffened cylindrical shells.

A comprehensive research review on more representative shell structure works conducted after 2000 has been reported by Zingoni [22]. The author collected and summarized over 70 more representative recent research on the vertical, horizontal, and different shell forms subjected to various environmental effects and loading types such as hydrodynamic, hydrostatic pressure, wind pressure, thermal effects, and seismic forces. The author concluded from this survey that research on metal shells continues to be dominated by any other shell forms.

Significant improvements in numerical solutions were made after computational advancement besides the above-mentioned experimental works. The finite element (FE) model can take the influence of geometric imperfections, material property variations, and thickness changes. The finite element model can accurately describe the boundary conditions, loading cases, structural detail features, and discrete stiffeners [2]; therefore, many researchers performed analytical analyses based on finite element methods. Using the finite element technique, Radha and Rajagopalan [23] studied the ring-stiffened pressure hull's inelastic buckling behavior. The authors performed numerical non-linear and buckling analyses to calculate the failure pressure. FE results exhibited good agreement with the classical methods. Temami [24] demonstrated the boundary condition effect on the stiffened and unstiffened cylindrical tank buckling strength. The numerical simulation was conducted by using commercially available ABAQUS code. Elsayed *et al.* [25] numerically investigated the optimum mesh size and best element type for both empty and liquid-filled circular cylindrical tanks. The authors performed mesh convergence studies with six element types available in the ANSYS library and addressed those parameters that can alter the results during finite element simulation. Tabish and Mamaghani [26] performed a numerical study to investigate the effect of height-to-diameter (H/R) and diameter-to-thickness (R/t) ratios on the axial buckling strength of the cylindrical shell. The authors proved that the critical axial buckling stress mainly depends on the slenderness ratio (R/t). Pasternak *et al.* [1] studied unstiffened and stiffened shell buckling behavior numerically and experimentally, using a series of small specimens, which were then used for further extensive parametric studies. These findings confirm that the ring-stiffeners can improve the thin-walled cylindrical shell buckling strength and postpone the ultimate buckling failure. Li *et al.* [27] continued the Pasternak work and examined ring-stiffened thin-walled cylindrical tank performance by analyzing cylindrical non-linear buckling strength. The authors tested the tank's performance experimentally and using finite element simulation. Stiffened and unstiffened models were manufactured, measuring imperfections with 3D scanning, Rhinoceros software, and MATLAB. The buckling load was obtained using an axial pressure measuring apparatus. Numerical imperfection geometries were modeled using ABAQUS/Explicit. The authors also suggested further parametric studies based on these experimental and simulated results, which can guide the ring-stiffened thin shells application in practice.

Cho *et al.* [28] examined possible failure modes for ring-stiffened cylinders and introduced a new interaction buckling failure mode. Nine geometrically imperfect models were manufactured, and failure modes were measured using an axial hydrostatic pressure apparatus. The authors proved experimentally that the failure modes are not limited only to the shell yielding, local shell buckling, and overall flexural buckling together with the stiffeners but also the interactive buckling with the combination of local and global buckling. Results were also validated by performing nonlinear FE analysis using the risk method from ABAQUS software. In addition, the authors proposed a simple criterion for differentiating these failure modes and pointed out the theoretical design equation deficiency that does not include interaction buckling failure mode. The authors suggested that more extensive experiments and numerical simulation generate a larger database for parametric studies, especially for further investigation of the interaction buckling phenomenon. Additionally, developing a new interaction design equation that includes interaction buckling behavior is needed. Although extensive research has contributed much to understanding the thin-walled stiffened-cylindrical shell buckling behavior; however, numerical works to investigate the stiffened-cylindrical shell buckling behavior based on stiffening properties variation are still rare. Therefore, a comprehensive numerical study is conducted with the aims to estimate and improve the buckling strength of the thin-walled cylindrical storage tanks under static loadings.

3 Finite Element Buckling Analysis of Unstiffened Cylinders Subject to Compressive Loading

This chapter presents a linear static analysis of finite element model to validate the overall performance and reliability of the model. This portion of the report has been submitted to a peer-reviewed conference for publication and is freely publicly available.

3.1 Preliminary Linear Elastic and Buckling Analysis

A linear elastic stress analysis was initially performed to verify the overall performance and quality of the numerical modeling approach, and computational analysis to calculate the linear buckling behaviour of empty cylindrical shells with different *H/D* and *D/t* ratios using commercial engineering software ANSYS workbench 2021 [29]. The theoretical results were compared with FE analysis results to substantiate the model.

3.2 Material Description and Geometry of the Cylindrical Tanks

Twelve different geometries of the tanks are analysed with height to diameter (H/D) ratios of 0.5, 1.0, 1.5, and 2.0 and the diameter to thickness (D/t) ratios of 1000, 1500, and 2000 to investigate the buckling behaviour of various sizes of the cylindrical tanks. These twelve cylindrical tanks are modeled as above-ground storage tanks open at the top, as shown in Figure 3-1. The material for all cylindrical storage tanks is steel with a modulus of elasticity, E = 200 GPa. ($29x10^6$ psi), Poisson's ratio, ν = 0.3. The geometries of the cylindrical tanks analyzed are listed in Table 3-1.

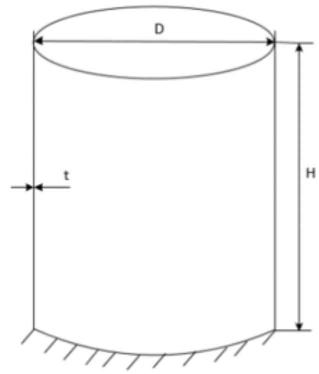

Figure 3-1. Cylindrical tank dimension

Table 3-1. Summary of twelve geometries of cylindrical shells

Model No.	*D*	*H*	*t*	*D/t*	*H/D*
1	9.144 m (360 in.)	4.573 m (180 in.)	9.144 mm (0.360 in.)	1,000	0.5
2	9.144 m (360 in.)	4.573 m (180 in.)	6.096 mm (0.240 in.)	1,500	0.5
3	9.144 m (360 in.)	4.573 m (180 in.)	4.572 mm (0.180 in.)	2,000	0.5
4	9.144 m (360 in.)	9.144 m (360 in.)	9.144 mm (0.360 in.)	1,000	1.0
5	9.144 m (360 in.)	9.144 m (360 in.)	6.096 mm (0.240 in.)	1,500	1.0
6	9.144 m (360 in.)	9.144 m (360 in.)	4.572 mm (0.180 in.)	2,000	1.0
7	9.144 m (360 in.)	13.716 m (540 in.)	9.144 mm (0.360 in.)	1,000	1.5
8	9.144 m (360 in.)	13.716 m (540 in.)	6.096 mm (0.240 in.)	1,500	1.5
9	9.144 m (360 in.)	13.716 m (540 in.)	4.572 mm (0.180 in.)	2,000	1.5
10	9.144 m (360 in.)	18.288 m (720 in.)	9.144 mm (0.360 in.)	1,000	2.0
11	9.144 m (360 in.)	18.288 m (720 in.)	6.096 mm (0.240 in.)	1,500	2.0
12	9.144 m (360 in.)	18.288 m (720 in.)	4.572 mm (0.180 in.)	2,000	2.0

3.3 Theoretical Buckling Stress for the Cylindrical Shell

The theoretical static buckling stress (σ_{cr}) for the cylindrical shells using the English unit is given by Timoshenko [30] theory of elastic stability is shown in Eq. (3.1),

$$\sigma_{cr} = \frac{E}{\sqrt{3(1-v^2)}}\left(\frac{t}{R}\right) \tag{3.1}$$

Where R is the radius of the cylindrical shell.

E is the modulus of elasticity.

t is the thickness of the cylindrical shell.

v is the Poisson's ratio.

3.4 Buckling Analysis of Cylindrical Shells using ANSYS:

The linear buckling analysis has been performed by using ANSYS workbench 2021. SHELL181 are adopted for all cylindrical shell geometries. SHELL181 has four nodes with 6 DOFs (i.e. 3 translations and 3 rotations) at each node. The SHELL181 is a 3-dimensional surface element and well-suited for analyzing thin to moderately-thick shell [31]. Based on the mesh convergence study, an optimum mesh size of 300 mm was selected for all models. The symmetry tool option was used in the Design Modeler window to reduce the computational time, as shown in Figure 3-2.

A simply supported boundary condition was applied by constraining all nodes at the top and bottom edges for all specimens; however, only axial displacement was allowed at the bottom edge. A Model No. 1 with loading and boundary conditions is illustrated as an example in Figure 3-3. For FEA buckling stress in ANSYS, the compressive pressure line of 1 N/mm was applied at the top to be a unit load, as shown in Figure 3-3. Thus, from ANSYS, the compressive pressure line of l N/mm multiplied by the multiplier is the critical value of buckling load. Figure 3-4 shows the Model No.1 ANSYS multiplier of 2218.3 N/mm.

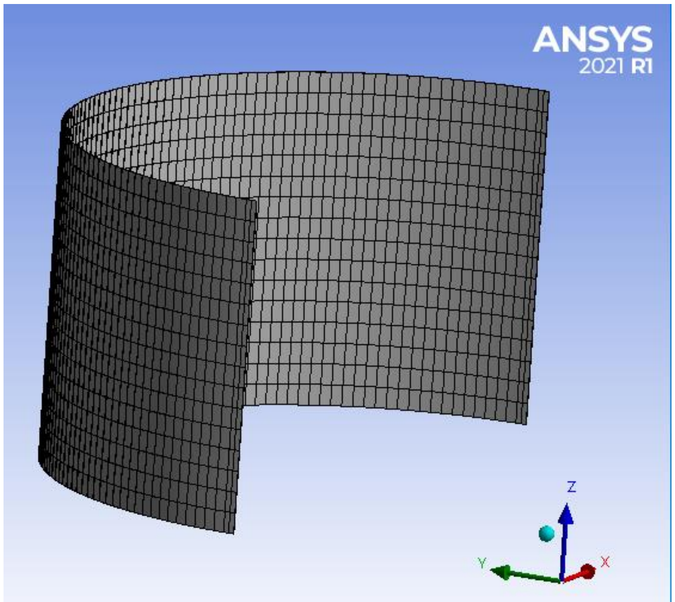

Figure 3-2. Model No.1 geometry in ANSYS Workbench

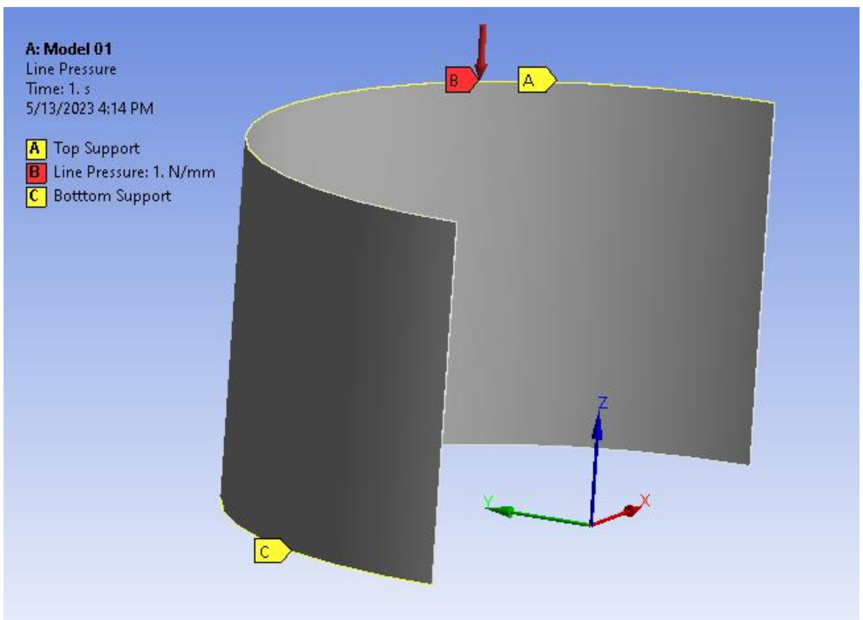

Figure 3-3. Model No. 1 compressive pressure line in ANSYS Workbench

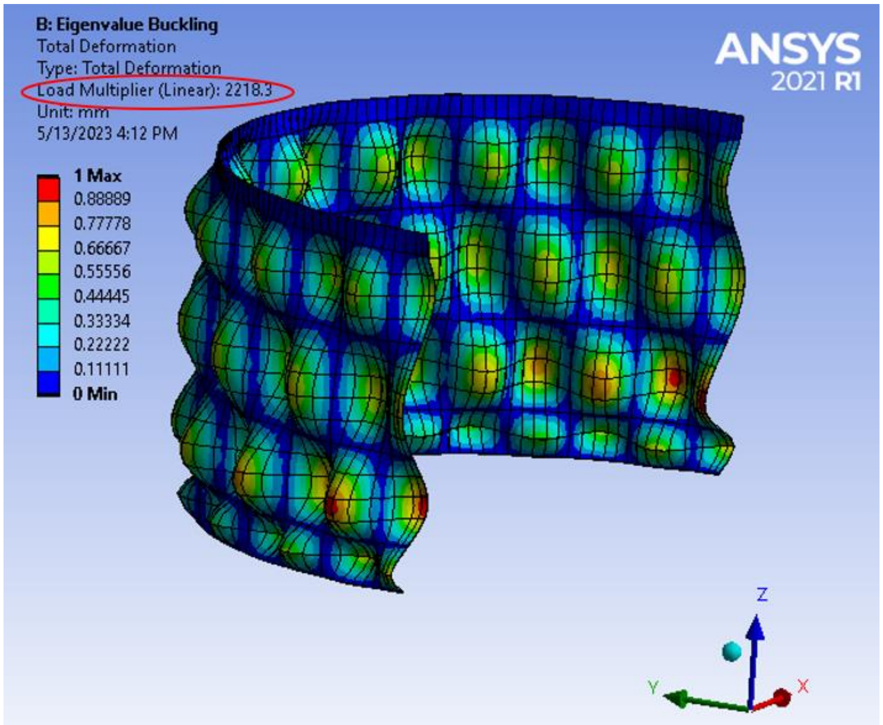

Figure 3-4. Model No.1 Buckling load multiplier

Calculations for Model No. 1 as an example are presented below to calculate the linear buckling stress values.

The theoretical, critical stress (σ_{cr})

$$\sigma_{cr} = \frac{E}{\sqrt{3(1-v^2)}}\left(\frac{t}{R}\right)$$

$$\sigma_{cr} = \frac{200000}{\sqrt{3(1-0.3^2)}}\left(\frac{9.144}{4573}\right) = 242.03 \text{ MPa}$$

and, the buckling stress from FEA by using ANSYS:

$$\sigma_{cr}(FEA) = \frac{\text{Multiplier}}{\text{t}} = \frac{2218.3}{9.144} = 242.60 \text{ MPa}$$

The comparison of FE axial buckling stresses with the theoretical values for all models is presented in Table 3-2. These results show that the critical compressive (buckling) stress mainly depends on the *D/t* ratio. The value of buckling stress decreases with the increase of the *D/t* ratio. These variations remain the same for any *H/D* ratio, as shown in Figure 3-5. In addition, FE results showed good agreement with theoretical values. These results show that the FEA models accurately predict static critical buckling stress. The solution of the buckling analysis provides multiple buckling mode shapes and critically buckling load values. Those mode shapes (eigenvectors) can indicate the expected buckling modes during the nonlinear analysis.

Table 3-2. Summary of results

Model No.	D (m)	H (m)	t (mm)	D/t	H/D	$\sigma_{cr.\ Theoretical}$ (MPa)	$\sigma_{cr.\ ANSYS}$ (MPa)
1	9.144	4.573	9.144	1,000	0.5	242.03	242.60
2	9.144	4.573	6.096	1,500	0.5	161.37	163.80
3	9.144	4.573	4.572	2,000	0.5	121.02	122.82
4	9.144	9.144	9.144	1,000	1.0	242.03	242.60
5	9.144	9.144	6.096	1,500	1.0	161.37	162.92
6	9.144	9.144	4.572	2,000	1.0	121.02	129.30
7	9.144	13.716	9.144	1,000	1.5	242.03	241.93
8	9.144	13.716	6.096	1,500	1.5	161.37	167.78
9	9.144	13.716	4.572	2,000	1.5	121.02	127.48
10	9.144	18.288	9.144	1,000	2.0	242.03	242.60
11	9.144	18.288	6.096	1,500	2.0	161.37	165.39
12	9.144	18.288	4.572	2,000	2.0	121.02	124.97

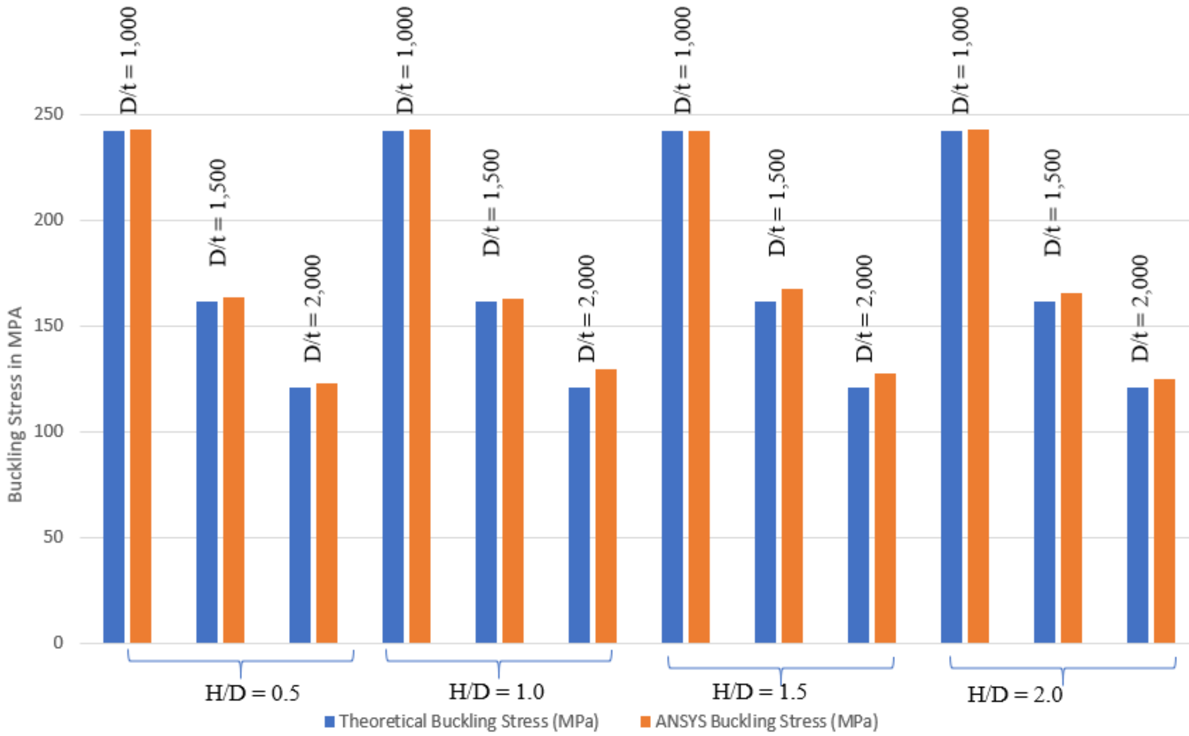

Figure 3-5. Comparison of FE axial buckling stresses with theoretical buckling stresses for all models

4 Numerical Buckling Behavior of Perfect and Imperfect Steel Cylinders Under External Pressure

4.1 Introduction

This chapter aimed to investigate the effect of *R/t* and *H/R* ratios and imperfections on the buckling strength of cylindrical tank specimens subjected to external pressure using the finite element technique. Twelve cylindrical tank specimens were considered with radius-to-thickness (*R/t*) ratios of 500 and 600, height-to-radius (*H/R*) ratios of 1.0 and 1.5, and imperfection depths of *4t* and *8t*. A linear and nonlinear buckling analysis using ANSYS workbench 2021 was conducted for all perfect and imperfect specimens to predict the critical buckling strength. The results are compared with the experimental results available in the literature and theoretical solutions. This portion of the report has been submitted to a peer-reviewed conference for publication.

4.2 Finite Element Modelling Description

4.2.1 Cylindrical Shell Geometries and Material Properties

Twelve cylindrical shell specimens categorized into four groups were considered based on the experimental work conducted by Fatemi *et al.* [32]. The first group is called Shallow Cylindrical Slim (SCS) specimen series and consists of three specimens SCSP, SCS4, and SCS8. The second group series, i.e., Deep Cylindrical Slim (DCS), consists of three specimens DCSP, DCS4, and DCS8. The third and fourth group series, Shallow Cylindrical Thick (SCT), and Deep Cylindrical Thick (DST), respectively, consist of three specimens each, i.e., SCTP, SCT4, SCT8, and DCTP, DCT4, DCT8. While P reparents perfect, 4 and 8 stand for *4t* and *8t* imperfection depth, where '*t*' is the shell thickness. The Depth of initial imperfection in imperfect test specimens measured in a circumferential direction is illustrated in Figure 4-2. The geometrical details for all cylindrical shell specimens, along with the size of dent tv for 4t and 8t specimens and the length of the curve l_{mQ} related to the *16t* and *32t* for imperfect test specimens, are listed in Table 4-1. The numerical geometries of perfect and imperfect specimens, along with their corresponding test images, are shown in Figure 4-1 as an example. Mild steel was used for all specimens with an ultimate strength Fu = 325.495 MPa, yield strength Fy = 194.238 MPa, modules of elasticity E = 200 GPa, and Poisson's ratio v = 0.28, obtained from the test specimen.

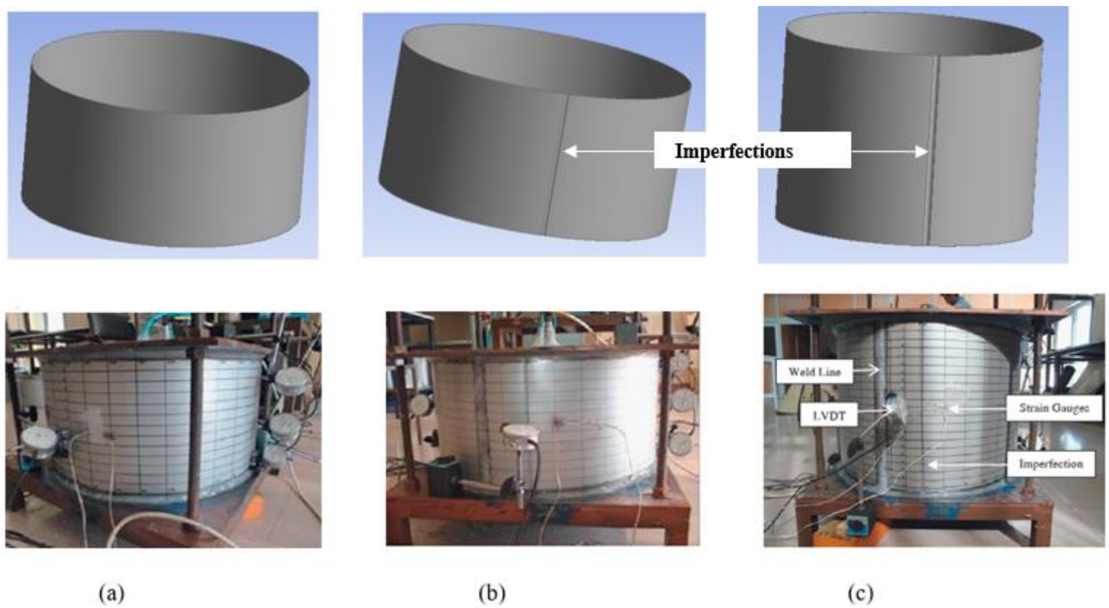

Figure 4-1. Numerical and test specimens (a) Perfect (b) 4*t* imperfect (c) 8*t* imperfect.

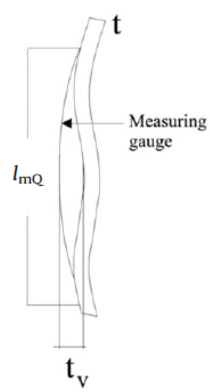

Figure 4-2. Depth of initial imperfection in tested specimens measured in a circumferential direction.

Table 4-1 Experimental specimen's dimensions.

Sr. No.	Specimen Name	Mode	R in mm	H in mm	t in mm	H/R	R/t	Size of dent (t_v) in mm	Length of curve (l_{mQ}) in mm
1	SCSP	Perfect	300	300	0.5	1.0	600	-	-
2	SCS4	4t	300	300	0.5	1.0	600	2	8
3	SCS8	8t	300	300	0.5	1.0	600	4	16
4	DCSP	Perfect	300	450	0.5	1.5	600	-	-
5	DCS4	4t	300	450	0.5	1.5	600	2	8
6	DCS8	8t	300	450	0.5	1.5	600	4	16
7	SCTP	Perfect	300	300	0.6	1.0	500	-	-
8	SCT4	4t	300	300	0.6	1.0	500	2.4	9.6
9	SCT8	8t	300	300	0.6	1.0	500	4.8	19.2
10	DCTP	Perfect	300	450	0.6	1.5	500	-	-
11	DCT4	4t	300	450	0.6	1.5	500	2.4	9.6
12	DCT8	8t	300	450	0.6	1.5	500	4.8	19.2

4.2.2 Element Type, Loading, and Boundary Conditions

SOLID187 is adopted for the cylindrical shell. SOLID187, illustrated in Figure 4-3, has ten nodes with 3 DOFs at each node [31]. All specimens were subjected to uniform external lateral pressure on the thin-walled cylindrical shell geometry. A simply supported boundary condition was applied by constraining all nodes at the top and bottom edges for all cylinders; however, only axial displacement was allowed at the top edge. A SCSP specimen with loading and boundary conditions is illustrated as an example in Figure 4-4.

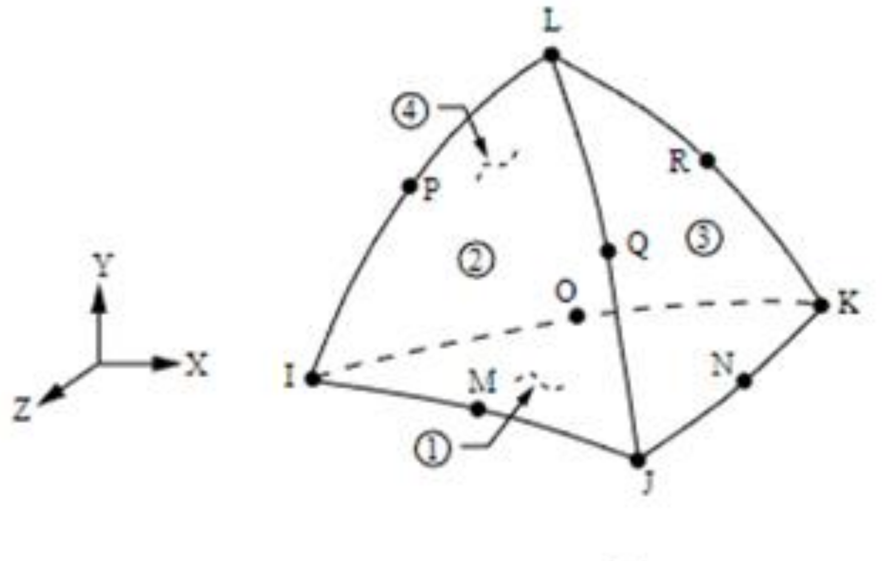

Figure 4-3. Element type: SOLID187 geometry

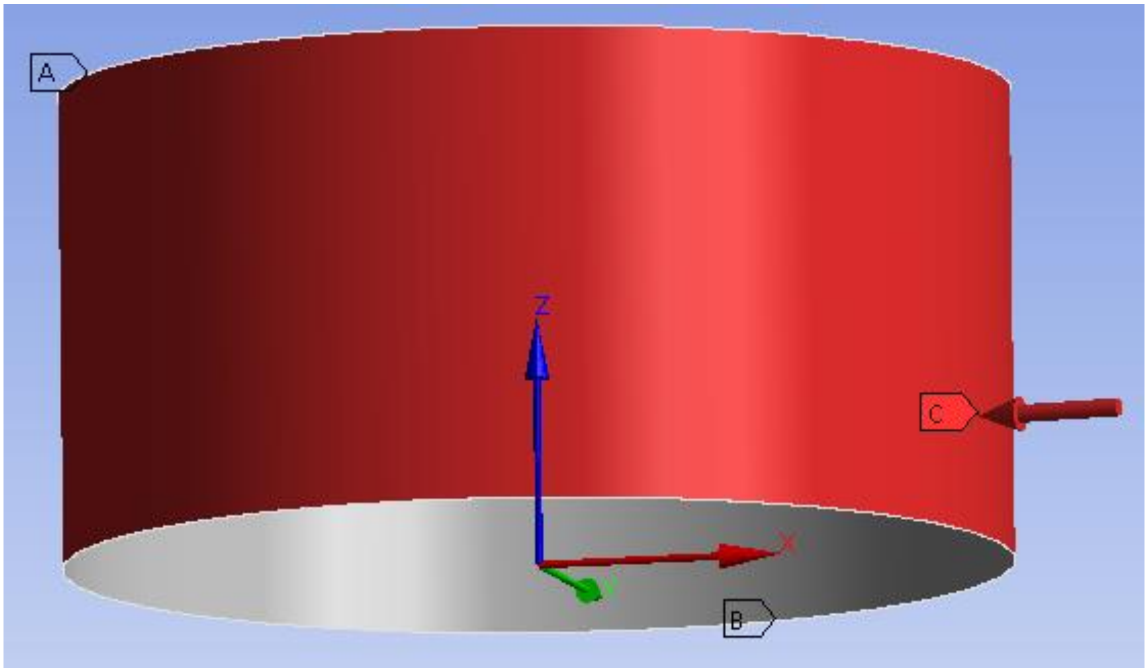

Figure 4-4. SCSP specimen geometry with loading and B.C.

4.3 Theoretical Buckling Pressure for Cylindrical Shell

Theoretical buckling pressure depends on the number of failure lobes *n*; therefore, the number of failure lobes is calculated by using the approximate Eq. (4.1) [32].

$$n = 2 \cdot 74\sqrt{\frac{R}{L}\sqrt{R/t}} \tag{4.1}$$

The theoretical formula in Eq. (4.2) to calculate linear buckling pressure for short and medium-long cylinders is given by R. Greiner [33].

$$P_{cr} = \sigma_u \frac{t}{R} \tag{4.2}$$

and

$$\sigma_u = \frac{E}{n^2}\left[\frac{1}{\left(1 + \left(\frac{n^2}{\pi^2}\right)(H / R)^2\right)^2} + \frac{(t / R)^2}{12(1 - \nu^2)}\left(n^2 + \pi^2\left(\frac{R}{H}\right)^2\right)^2\right] \tag{4.3}$$

Where,

σ_u is the critical or ultimate circumferential stress.

ν = Poisson's ratio

E = Modulus of Elasticity (MPa)

R = Shell inner radius (mm)

t = Shell thickness (mm)

H = Cylindrical shell Height (mm)

n = Number of circumferential waves or lobes

4.4 Numerical Buckling Analysis

4.4.1 Linear Buckling Analysis

A linear buckling analysis was conducted for perfect cylindrical specimens to predict the critical buckling strength. Linear analysis was performed using ANSYS workbench 2021, and a uniform pressure of 1 MPa was applied normally to the cylindrical longitudinal axis. The final critical buckling pressure was achieved by multiplying the unit pressure by the multiplier obtained after the simulation. The FE results were compared with the experimental works by Fatemi *et al.* [32] and the theoretical design formula available in codes.

4.4.2 Mesh Convergence Study

The final critical buckling pressure and the number of circumferential lobes at failure depend on the FE mesh size, as indicated in Table 4-2 for specimen SCSP; therefore, a mesh convergence study was essential to ensure that the final solution is independent of the mesh size. This mesh independence study was conducted for all perfect specimens to ensure that there is no need for further mesh refinement for FE results accuracy. Figure 4-5 illustrates the mesh convergence study for all perfect specimens. The mesh convergence study indicates a steady state and almost unaffected buckling results after a certain level of mesh refinement for all specimens. Based on the mesh convergence study, an optimum mesh size of 15 mm was selected for all specimens for further analysis.

Table 4-2. Element mesh size Vs. FE results for specimen SCSP

Element Size	No. of Elements	No. of Lobes	FE Buckling Pressure in kPa	% Pressure Difference
30	5292	10	31.17	-
25	7600	10	28.23	9.41
20	11780	11	27.22	3.58
15	20664	11	26.58	2.36
10	23058	15	26.18	1.50

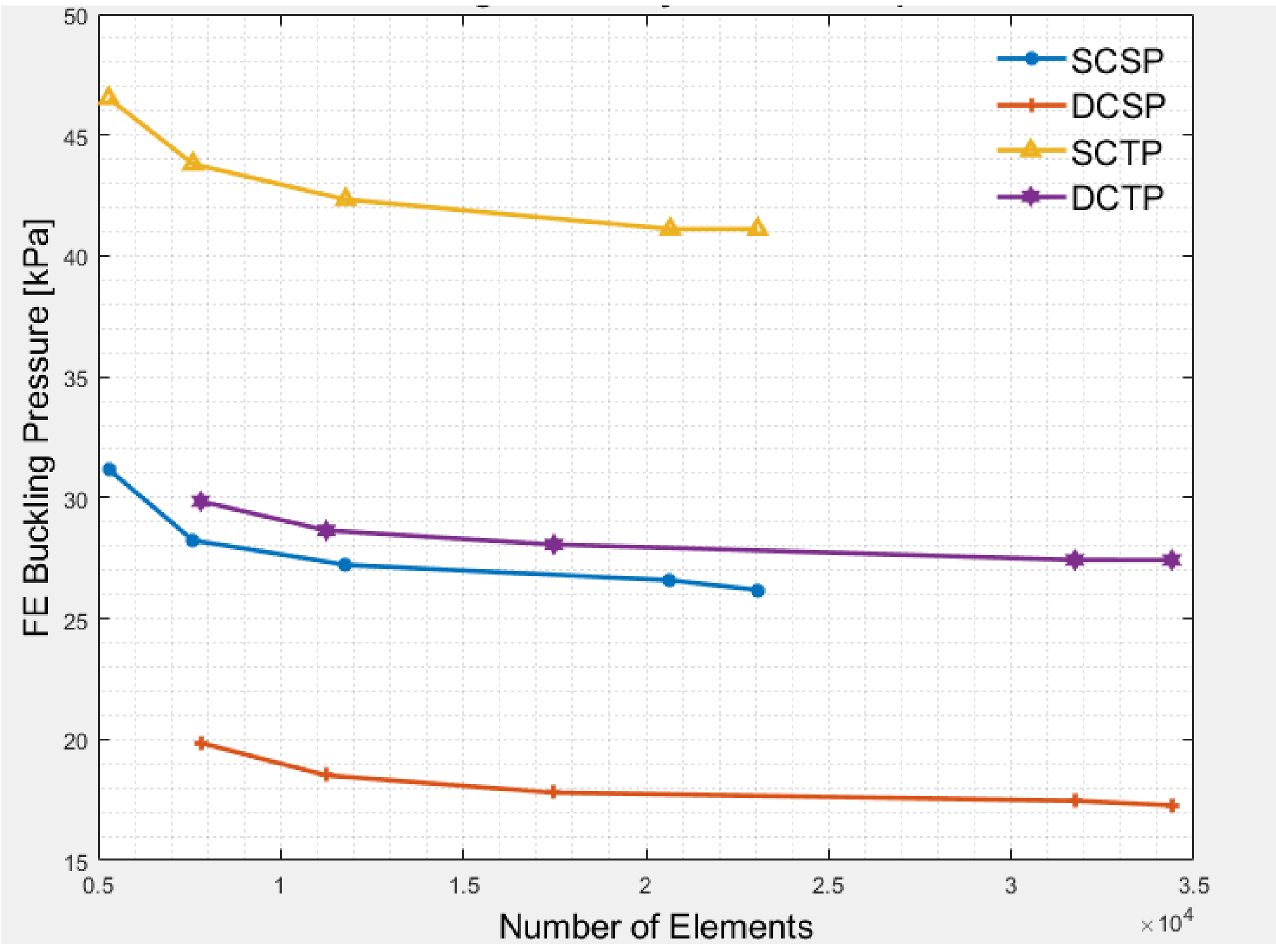

Figure 4-5. Mesh convergence for perfect specimens

4.4.3 Linear buckling analysis compare with experimental and analytical results

This section compares the linear buckling pressure obtained from the FEA to the experimental results obtained by Fatemi *et al*. [32] and theoretical buckling pressure based on approximate number of circumferential lobes. The critical buckling results along with circumferential lobes at failure for perfect specimens are summarized in Table 4-3.

Table 4-3. Results summary for perfect specimens.

Sr. No.	Specimen No.	Experimental Buckling Pressure (kPa)	FE Buckling Pressure (kPa)	Theoretical Buckling Pressure (kPa)
1	SCSP	28.57 (10)	28.23 (10)	20.86 (13)
4	DCSP	14.13 (8)	18.52 (12)	13.91 (11)
7	SCTP	38.71 (10)	41.11 (11)	32.91 (12)
10	DCTP	18.38 (8)	27.43 (12)	21.94 (10)

The value inside (), shows the number of circumferential lobes at failure.

4.4.4 Non-Linear Buckling Analysis

All imperfect specimens with 4*t* and 8*t* imperfections were analyzed using nonlinear analysis. ANSYS workbench 2021 performed nonlinear buckling analysis using the Newton-Raphson method [34]. An SCS8 specimen geometry with loading and FE failure shape, along with its corresponding test image, is shown in Figure 4-6 as an example. It was observed that the buckling waves were formed in the middle of the shell height with maximum displacement at the center and failure line located approximately over the imperfection location, similar to the test observations. The load-deformation curve at the location of maximum nodal deflection for all imperfect specimens is illustrated in Figure 4-7.

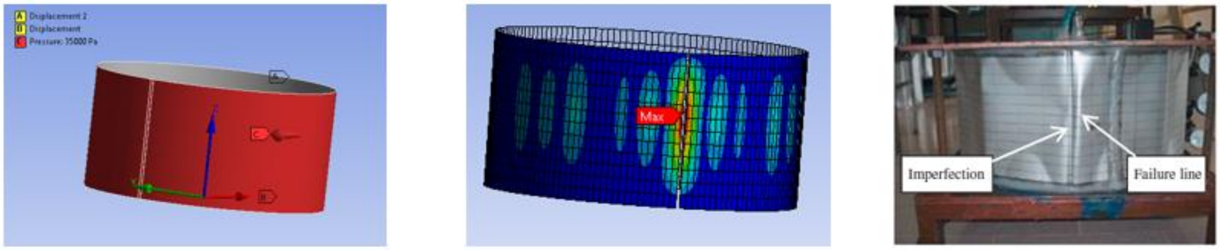

(a) (b) (c)

Figure 4-6. SCS8 (a) Geometry with Loading (b) FE failure shape (c) Test image at failure.

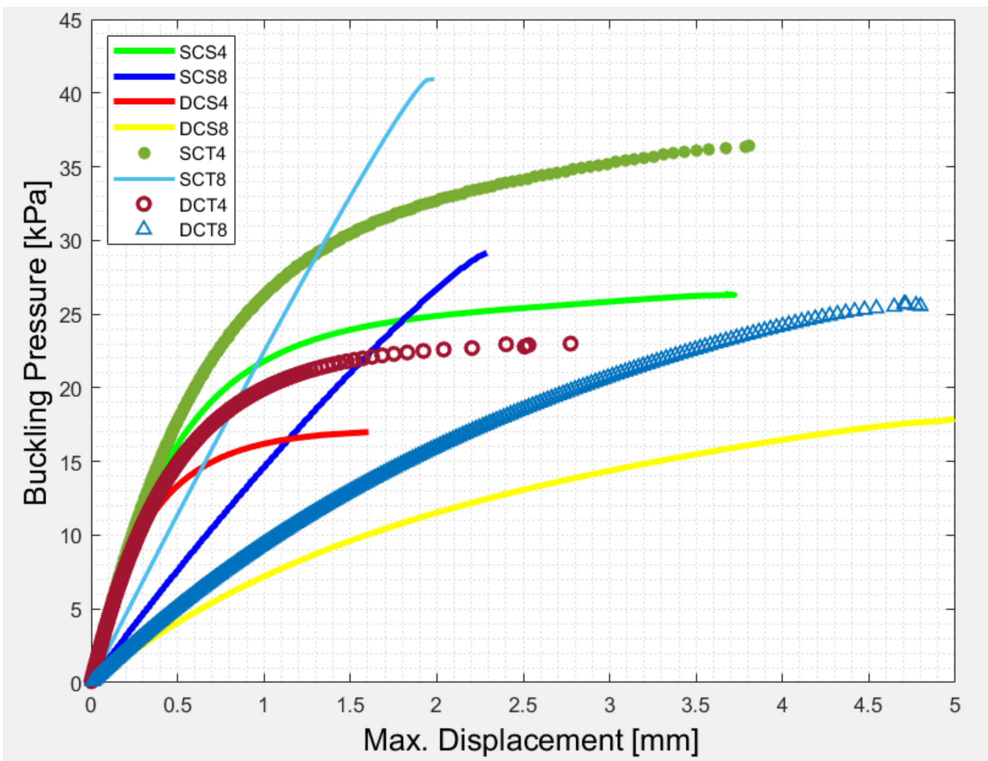

Figure 4-7. Load-deflection curve at the location of maximum nodal deflection for all imperfect specimens

Experimental and FE non-linear failure result comparison for all imperfect specimens is illustrated in Table 4-4.

Table 4-4. Experimental Vs. FE non-linear buckling pressure for imperfect specimens.

Sr. No.	Specimen No.	Experimental Buckling Pressure (kPa)	FE Buckling Pressure (kPa)
2	SCS4	27.95	26.40
3	SCS8	33.98	29.15
5	DCS4	17.58	17.00
6	DCS8	17.83	17.90
8	SCT4	29.30	36.45
9	SCT8	30.60	40.95
11	DCT4	19.70	23.00
12	DCT8	20.43	25.70

4.4.5 Results Discussion and Conclusion

The comparison of FE linear and nonlinear analysis with the experimental and theoretical values for all specimens is presented in Figure 4-8. These results show that varying *R/t* and *H/R* ratios strongly influence the critical buckling pressure. The buckling pressure remarkably increases with the decrease of both *R/t* and *H/R* ratios; however, the effect of the *R/t* ratio is more dominant than the *H/R* ratio. The Results revealed that the geometric imperfections have little influence on the overall buckling capacity, especially for tanks with large *H/R* ratios and smaller *R/t* ratios. Numerical results show good agreement with experimental and theoretical results; however, FEA gave higher results, especially for cylinders with smaller *R/t* ratios might be due to neglecting imperfections that are probably created in the construction process. It is concluded that the finite element technique can be adapted to generate a larger database for further numerical studies based on varying parameters.

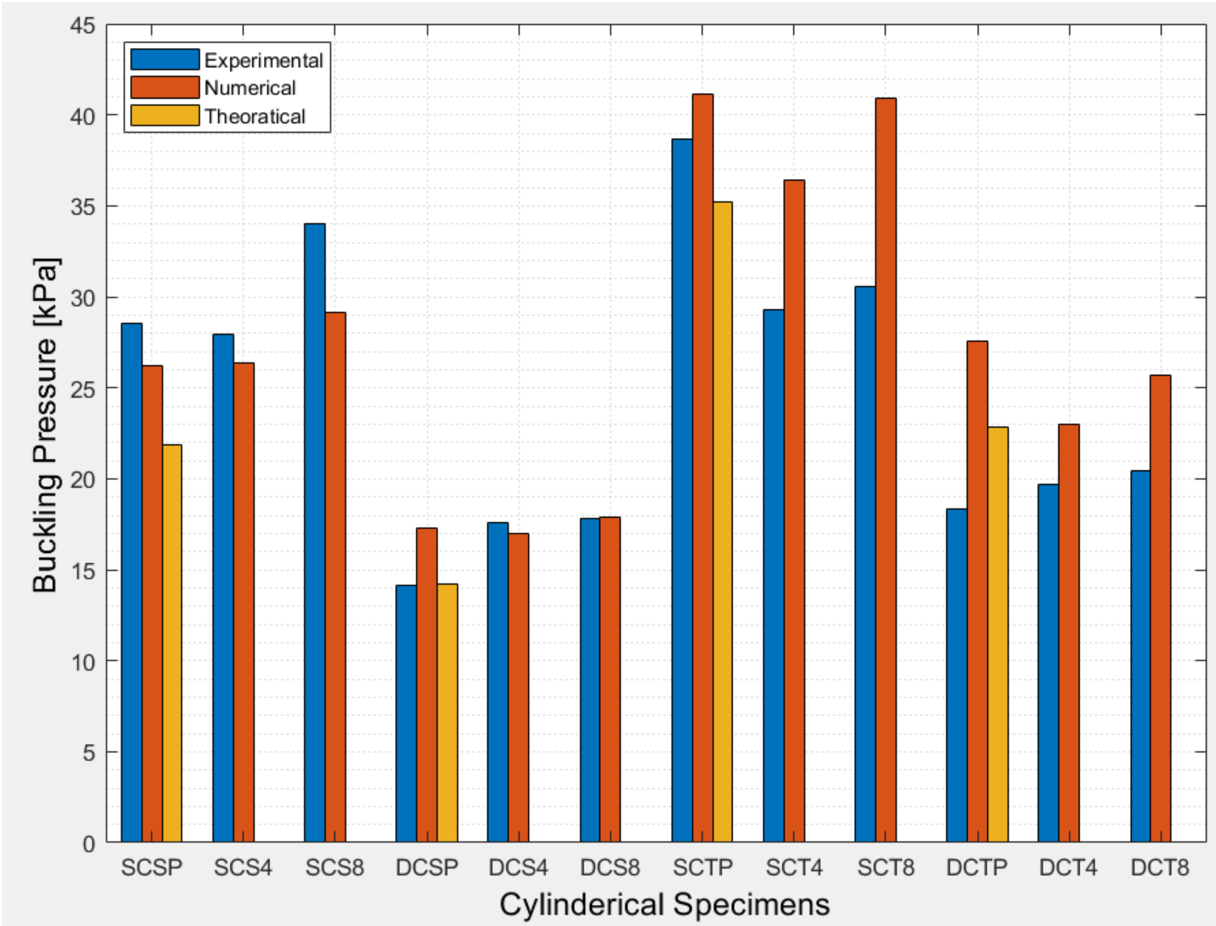

Figure 4-8. Comparison of FE buckling pressures with exp. and theoretic results for all specimens.

5 Buckling Behavior of Thin-Walled Stiffened-Aluminium Cylindrical Shells Subjected to External Lateral Pressure

5.1 Introduction

Ring stiffeners are preferably used to enhance thin-walled cylindrical shell buckling resistance while subjected to external lateral pressure. This chapter aims to investigate the influence of external ring stiffeners varying from 3 to 17 on a thin-walled, stiffened aluminium cylindrical shell buckling strength. Ten ring-stiffened cylindrical specimens were modeled using an ANSYS workbench whose stiffener dimensions varied so that all specimens' overall weight remained constant. FE linear and nonlinear buckling results were compared with the experimental work and the theoretical formulas in the literature. The failure mode shapes and number of circumferential lobes at failure for all specimens obtained from the linear analysis closely matched the experimental failure pattern. The linear buckling pressures were lower than the corresponding experimental critical pressures; however, they compare well with the buckling pressure obtained from the theoretical equations. The nonlinear buckling pressures for perfect geometries are lesser than the experimental pressures, and specimens with nine or fewer stiffeners were crushed instead of buckling at failure. For nonlinear analysis of imperfect geometries based on the eigenmode shape, results revealed that the 5 % imperfection giving the failure mode shapes similar to the experimental buckling shapes for most of the specimens, and local shell buckling pressures were closer to the experimental buckling pressures compared to the overall flexural buckling results. The overall FE results indicate that the failure mode types shifted from shell local buckling mode to the flexural buckling mode while increasing the number of ring stiffeners by keeping the specimen's overall weight constant. Parametric study reveals that linear and nonlinear buckling strength remarkably improved by keeping a constant stiffener height compared to the FE buckling strength for specimen dimensions obtained from experiments, especially for specimens that failed with overall flexural buckling mode. The experimental, theoretical, and finite element (FE) results proved that the ring stiffener's optimum size and spacing could improve the stiffened cylinder buckling strength since critical buckling pressure and failure mode shape were influenced by the ring stiffener's size and spacing. This portion of the report has been submitted to a peer-reviewed journal for publication and will be accessible publicly upon acceptance.

5.2 Finite Element Modelling

5.2.1 Stiffened Shells Geometry and Material Properties

In this study ten aluminium-made stiffened cylindrical shells under external pressure, with ring stiffeners varying from 3 to 17, tested by Seliem and Roorda [16] are analysed to investigate the ring stiffener's effect on buckling mode and buckling pressure. The geometrical details for all ring-stiffened cylindrical shells analysed are listed in Table 5-1. Table 5-1 shows that the specimen No. 2, 3, and 7 were repeated with 9, 10 and 8 respectively; therefore, FE analysis were conducted for specimen No. 1 to specimen No. 7. The geometry stiffened cylindrical shell for specimen No. 4 is presented in Figure 5-1 as an example. All specimens had the same inner radius R = 127 mm (5 in.), overall shell length L = 889 mm (35 in.), and shell thickness t = 2.0 mm (0.08 in.). Cylindrical shells are mainly categorised into three length domains namely short, medium, and long during the design process [35], [36]. The Batdorf [37] parameter (Z) in Eq. (5.1) considered to categorizes the cylindrical shell type.

$$Z = \frac{l^2}{Rt^2}\sqrt{1 - v^2} \tag{5.1}$$

Where,

l = Cylinderical shell length between two ring stiffeners in mm

R = Inner shell radius in mm

t = Shell thickness in mm

υ = Poisson ratio

Since the Batdorf parameter depends on the square of the length between the stiffeners or boundaries; therefore, it can take a very large value for long cylinders (i.e Z > 4000). Short cylinders having low Batford Parameter (i.e Z < 100). The cylindrical shell is considered a medium-length cylinder if lies in-between 100 < Z < 4000 [2]. Batford parameter for the present study listed in Table 5-1 indicates that all specimens are categorized in short and medium-long cylinders. The size, spacing, and number of stiffeners were varied so that the overall weight for all specimens remained constant at 6.57 kg (14.5 lb). Aluminum alloy 6061 was used for both rings and cylinders with an ultimate tensile strength F_u = 262 MPa (38,00 psi), yield strength F_y= 241 MPa (35,000 psi), modules of elasticity E = 71000 MPa (10.298 x 10^6 psi) and Poisson's ratio v = 0.33, obtained from the test specimen.

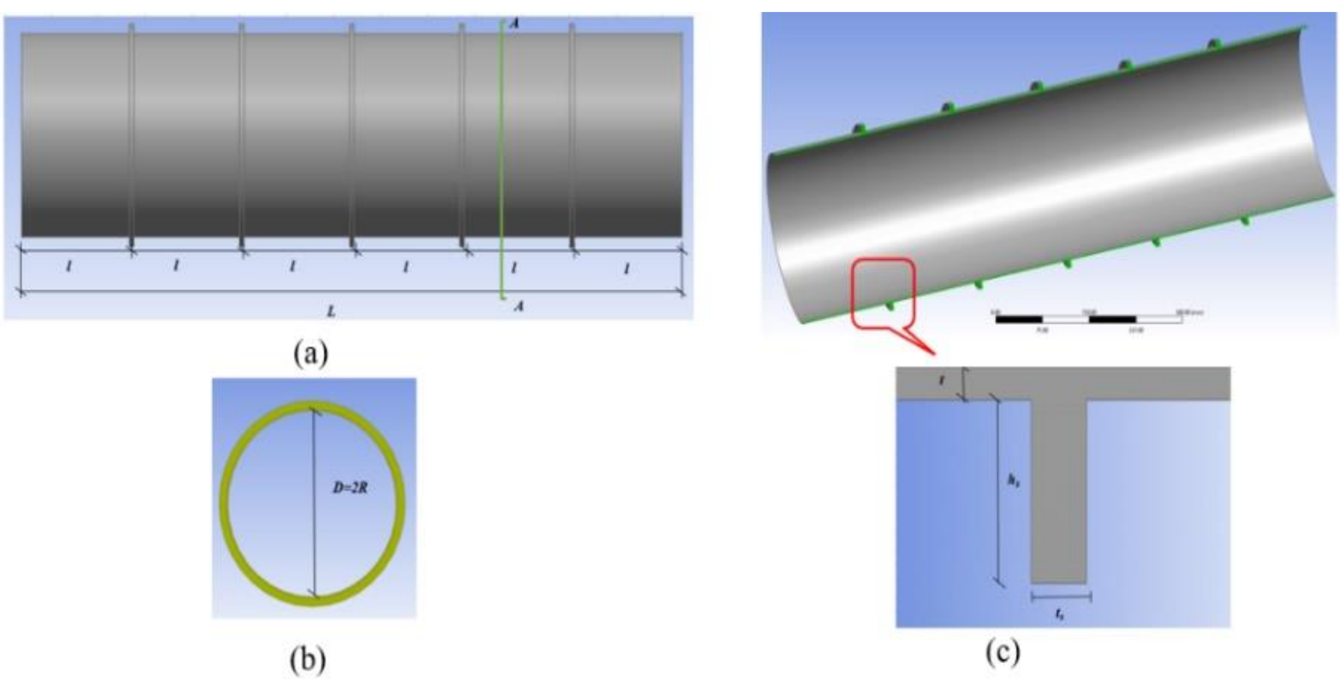

Figure 5-1. Specimen No. 4 (a) Longitudinal view (b) Section AA (c) Stiffener cross-sectional view

Table 5-1. Experimental specimens' dimensions.

Specimen No.	No. of Stiffeners (N)	Stiffener Spacing (l) in mm	Stiffener Thickness (t_s) in mm	Stiffener Height (h_s) in mm	Batdorf or Curvature Parameter (Z)
1	17	49.39	3.56	7.37	9.06
2	3	222.25	8.64	17.27	183.57
3	13	63.50	4.06	8.38	14.98
4	5	148.17	6.60	13.46	81.59
5	11	74.08	4.57	9.14	20.39
6	7	111.13	5.59	11.43	45.89
7	9	88.90	5.08	9.91	29.37
8	9	88.90	5.08	9.91	29.37
9	3	222.25	8.64	17.27	183.57
10	13	63.50	4.06	8.38	14.98

5.2.2 Meshing and Element Type

All ring stiffened cylindrical specimens meshed as a 3D surface body with SHELL181 element type. A quadrilateral mesh size of 13 mm adopted for both rings and shell geometries for all specimens based on the mesh convergence study. A ring-stiffened specimen No. 5 with meshing is illustrated as an example in Figure 5-2.

SHELL181, illustrated in Figure 5-2 has four nodes with 6 DOFs (i.e., 3 translations and 3 rotations) at each node. The SHELL181 is a 3-dimensional surface element and well-suited for analysing thin to moderately thick shell structures [31].

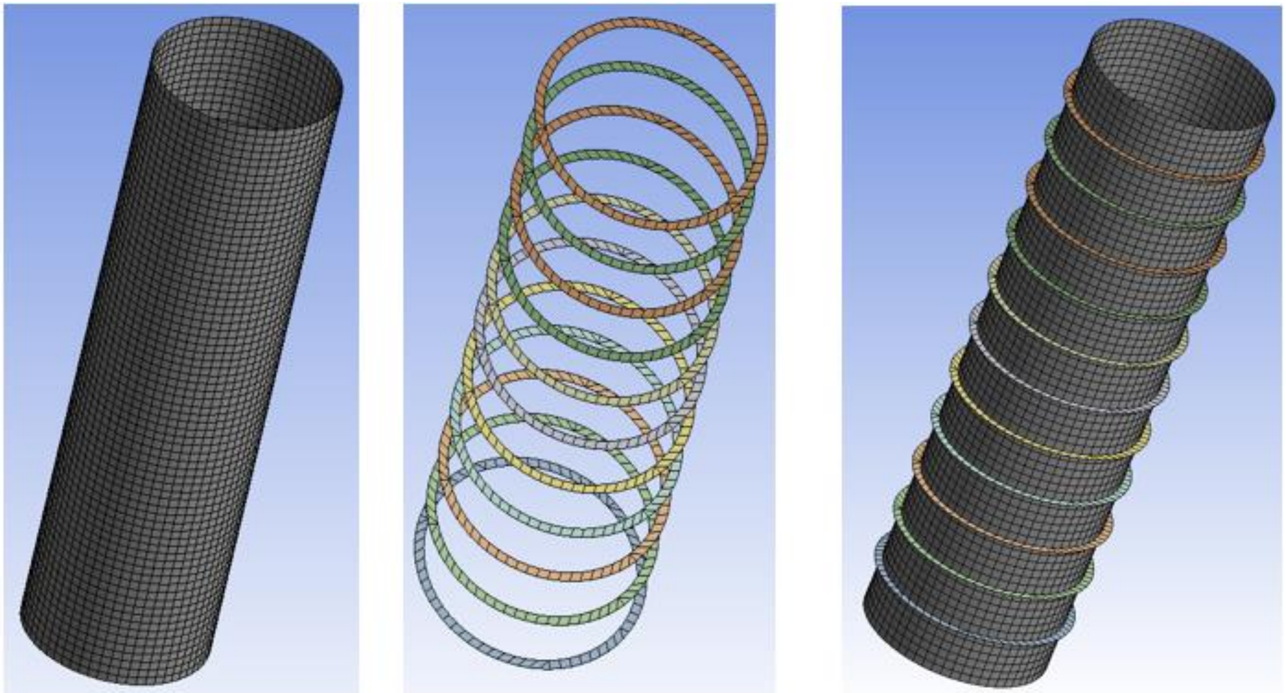

(a)

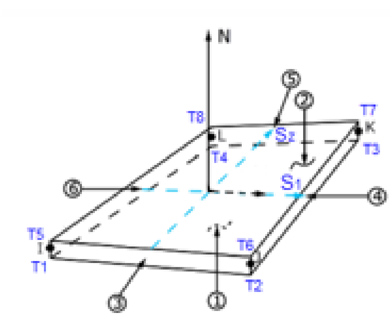

(b)

Figure 5-2. Specimen No. 5 (a) Meshing (b) SHELL181 geometry

5.2.3 Loading, and Boundary Conditions

All specimens were subjected to uniform external pressure applied normally to the cylindrical longitudinal axis. A simply supported boundary condition was applied by constraining all nodes at the top and bottom edges for all specimens; however, only axial displacement was allowed at the bottom edge. A ring-stiffened specimen No. 5 with loading and boundary conditions is illustrated as an example in Figure 5-3.

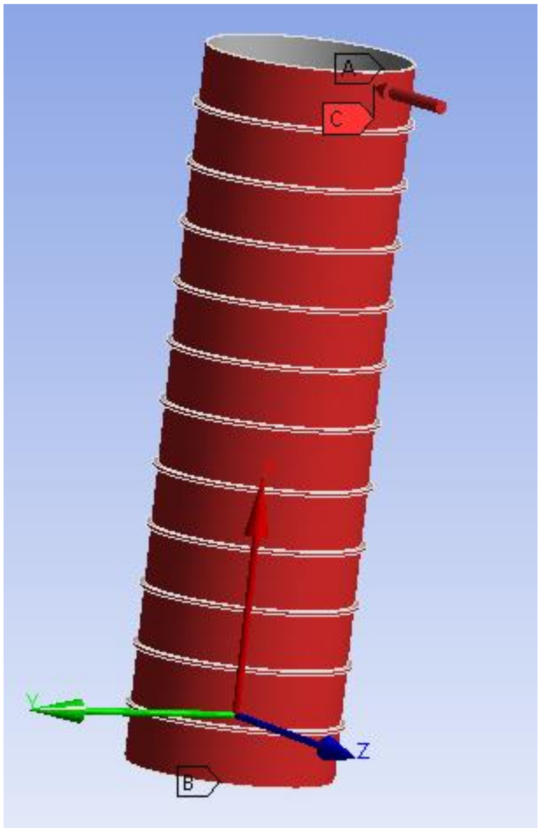

Figure 5-3. Specimen No. 5 geometry with loading and B.C

5.3 FE Linear Analysis

A linear analysis was conducted for all ring-stiffened cylindrical specimens to predict the critical buckling strength. Linear analysis can give anticipated buckling mode shapes (eigenvectors) and adequate finite element mesh to represent that failure pattern [38]. Linear analysis (LA) was performed using ANSYS workbench 2021, and a uniform pressure of 1 MPa was applied normally to the cylindrical longitudinal axis. A load multiplier was obtained after the linear analysis completion. The critical buckling pressure was achieved by multiplying the unit pressure by this multiplier.

The FE results were compared with the experimental works by Seliem and Roorda [16] and the theoretical design formulas available in codes.

5.3.1 Mesh Convergence Study

The critical buckling pressure and the number of circumferential lobes at failure depend on the FE mesh size, as indicated in Table 5-2 and Table 5-3 for specimens No. 1 and 2, respectively, as an example of both types of failure; therefore, a mesh convergence study was essential to ensure that the final solution is independent of the mesh size. This mesh independence study was conducted for all specimens to ensure that the FE failure lobes were closely matched with experimental failure lobes and that there is no need for further mesh refinement for FE results accuracy. Figure 5-4 illustrates the mesh convergence study for all specimens. The mesh convergence study indicates a steady state and almost unaffected buckling results after a certain level of mesh refinement for all specimens. Based on the mesh convergence study, an optimum mesh size of 13 mm was selected for all specimens for further analysis.

Table 5-2. Element mesh size Vs. FE results for specimen No. 1

Element Size (mm)	No. of Elements	Circumferential Lobes at Failure	FE Linear Buckling Pressure (MPa)	% Pressure Difference
30	1497	2	2.49	-
20	3065	3	2.09	16.06
15	4189	3	2.07	0.96
13	5497	3	2.04	1.55
10	8628	3	2.01	1.37
8	14403	3	2.00	0.50

Table 5-3. Element mesh size Vs. FE results for specimen No. 2

Element Size (mm)	No. of Elements	Circumferential Lobes at Failure	FE Linear Buckling Pressure (MPa)	% Pressure Difference
30	981	4	1.84	-
20	2015	5	1.56	15.13
15	3423	6	1.47	5.45
13	4606	6	1.45	1.76
10	7873	6	1.42	2.28
8	12298	6	1.40	1.13

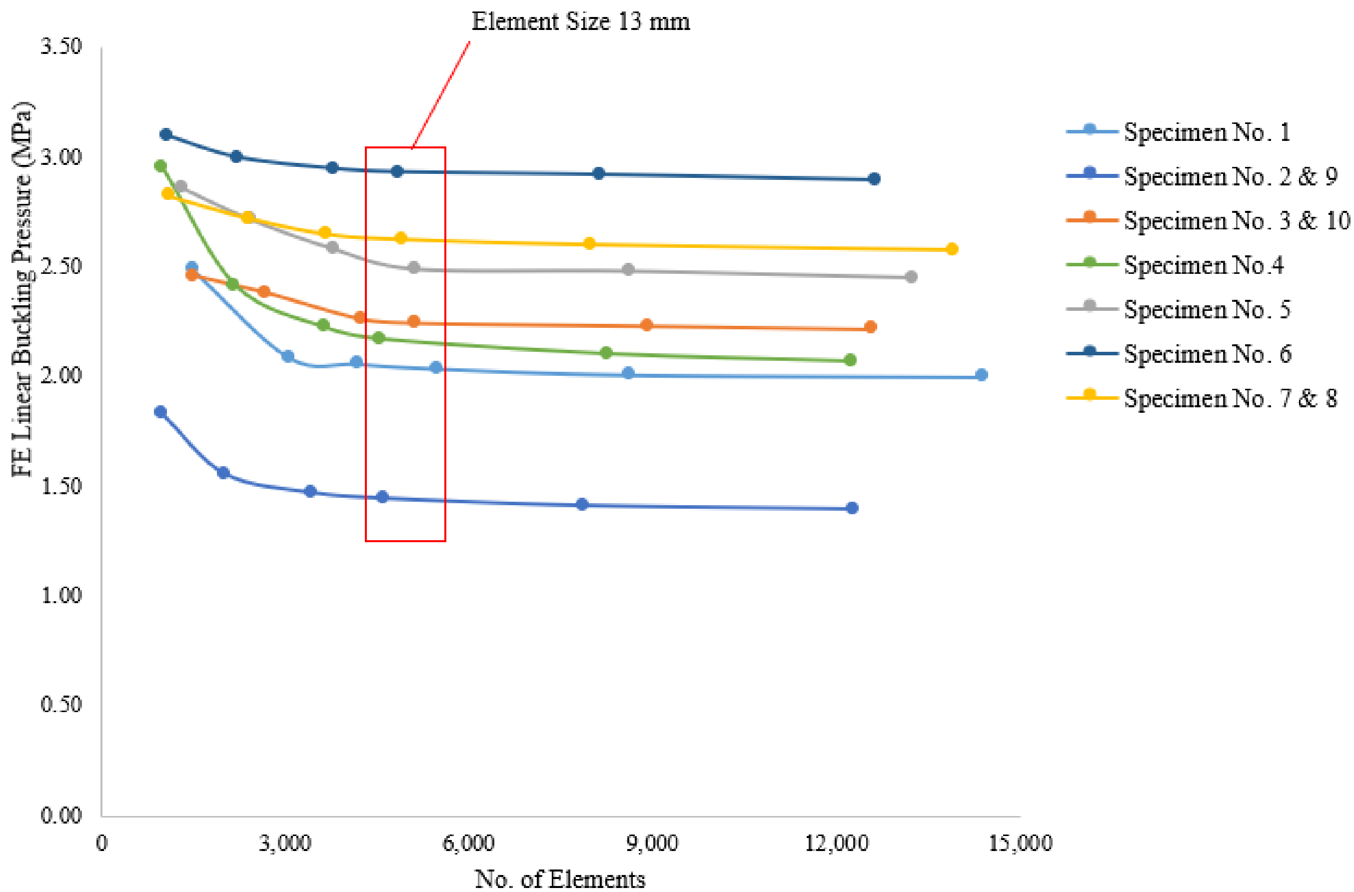

Figure 5-4. Mesh convergence for all specimens

5.3.2 Linear Analysis Compare with Analytical Solution

This section compares the linear buckling pressure obtained from the FEA to the analytical buckling pressure. Theoretical buckling pressure depends on the number of failure lobes *n*; therefore, theoretical buckling pressure was calculated using the same number of circumferential lobes observed during the experimental work.

The finite element buckling pressure P_{cr} for perfect ring stiffened cylinders that failed in overall flexural buckling mode is compared with the widely used theoretical formula in Eq. (5.2) based on Bryant's [8] and Kendrick's [5] solution.

$$P_{cr} = \frac{Eh_s}{R} \frac{\pi^4 R^4/L^4}{\left(n^2 + \frac{\pi^2 R^2}{2L^2} - 1\right)\left(n^2 + \frac{\pi^2 R^2}{L^2}\right)^2} + \frac{EI_e(n^2 - 1)}{l\Omega} \tag{5.2}$$

In the case of Bryant's and Kendrick's solution, Ω is given in Eq. (5.3) and Eq. (5.4) respectively.

$$\Omega = \left(R + \frac{h_s}{2}\right)(R + e_s)^2 \tag{5.3}$$

$$\Omega = R^3 \tag{5.4}$$

Where,

P_{cr} = Critical buckling pressure (MPa)

N = Number of ring stiffeners

L = Cylindrical shell overall length (mm)

R= Inner shell radius (mm)

n = Number of circumferential waves or lobes

E = Modulus of elasticity (MPa)

e_s = Stiffeners eccentricity

I_e = Centroidal moment of inertia of the effective section comprising one stiffener plus an effective shell width (mm^4)

h_s = Stiffener height (mm)

l = Cylinderical shell length between two ring stiffeners (mm)

The FE linear buckling pressure P_{cr} for perfect ring stiffened cylinders that failed in local shell buckling mode are compared with the theoretical formula in Eqs. (4.2 & 4.3) for short and medium-long cylinders given by R. Greiner [33].

The critical buckling results from the above-mentioned theoretical formula and the FE linear buckling analysis obtained for cylindrical specimens failing by the overall flexural buckling mode are summarized in Table 5-4, while the results for cylindrical specimens failing by the local shell buckling mode are presented in Table 5-5.

Table 5-4. FE Vs. Theoretical buckling pressure for OFBM

Specimen No.	Number of Stiffeners	FE Linear Buckling Pressure (MPa)	Bryant Buckling Pressure (MPa)	Kendrick Buckling Pressure (MPa)
1	17	2.04	2.03	2.11
3 & 10	13	2.25	2.31	2.42
5	11	2.49	2.59	2.74
7 & 8	9	2.63	2.84	3.01

Table 5-5. FE Vs. Theoretical buckling pressure for LSBM

Specimen No.	Number of Stiffeners	FE Linear Buckling Pressure (MPa)	R. Greiner Buckling Pressure (MPa)
2 & 9	3	1.45	1.32
4	5	2.18	2.06
6	7	2.93	3.65

5.3.3 Linear Analysis Compare with Experimental Results

In this section, linear analysis results compared with the experimental results obtained by Seliem and Roorda [16] are briefly discussed for each specimen. Seliem and Roorda [16] calculated the critical buckling pressure from the experimental results obtained from the geometrically imperfect ring-stiffened cylindrical shells using the Southwell method [39]. Seliem and Roorda [16] used the Southwell method using Fourier amplitude corresponding to the experimental buckling modes. Although this method gives overestimated results for certain cylindrical buckling problems [40]

[41]; however, it was used in the experimental study because of its consistency and ease of application.

Experimental and FE linear analysis result could be categorized into three types. The first category stiffened cylinders with lighter ring stiffeners (i.e., specimen No. 1,3 and 10) failed in the overall flexural mode without the influence of the other mode. The second type of stiffened cylinders with strong rings (i.e., specimen No. 2,4 and 9) failed in the local shell mode with no influence of the overall flexural failure mode. The third type stiffened cylindrical specimens (i.e., specimen No. 5,6,7 and 8) failed with interactive buckling mode mixed with local and overall flexural buckling. The specimens in the third category were failed with primary mode (one of the two possible modes); however, the secondary mode influenced the final failure shape. Experimental and FE linear buckling result comparison for all specimens is illustrated in Table 5-6.

Linear analysis results in Table 5-6 indicate that the failure mode shapes for all specimens closely matched the experimental failure pattern. FE linear buckling pressures for local shell buckling mode are closer to the corresponding experimental critical pressures; however, FE buckling pressures for overall flexural buckling mode varies from the critical buckling pressures obtained for the experimental data.

Table 5-6. Experimental Vs. FE linear buckling pressure

Sr. No.	No. of Stiffeners	Specimen No.	Critical Buckling Pressure Obtained from Experiment (MPa)	FE Linear Buckling Pressure (MPa)	Experimental Lobes at Failure	FE Lobes at Failure	Failure Mode
1	3	2	1.61	1.45	6	6	LSBM
2		9	1.26		6		
3	5	4	2.36	2.18	8	7	LSBM
4	7	6	3.60	2.93	8	6	Interactive but dominant with LSBM
5	9	7	4.06	2.63	8	3	Interactive but dominant with LSBM
6		8	3.58		3		Interactive but dominant with OFBM
7	11	5	3.28	2.49	3	3	Interactive but dominant with OFBM
8	13	3	2.96	2.25	3	3	OFBM
9		10	3.17		3		
10	17	1	3.03	2.04	3	3	OFBM

Overall flexural buckling mode

Specimen No. 1 had a 17-maximum number of ring stiffeners that failed in the overall flexural buckling mode with three failure lobes initiating from the middle bay and extending over the entire cylindrical length representing failure patterns similar to the experimental work as illustrated in Figure 5-5. The largest deformation before buckling was observed at the middle bey and radial deformation shape was similar to the experimental circularity contours before failure as illustrated in Figure 5-6. The FE linear buckling pressure is 2.04 MPa compared to the experimental critical pressure of 3.03 MPa.

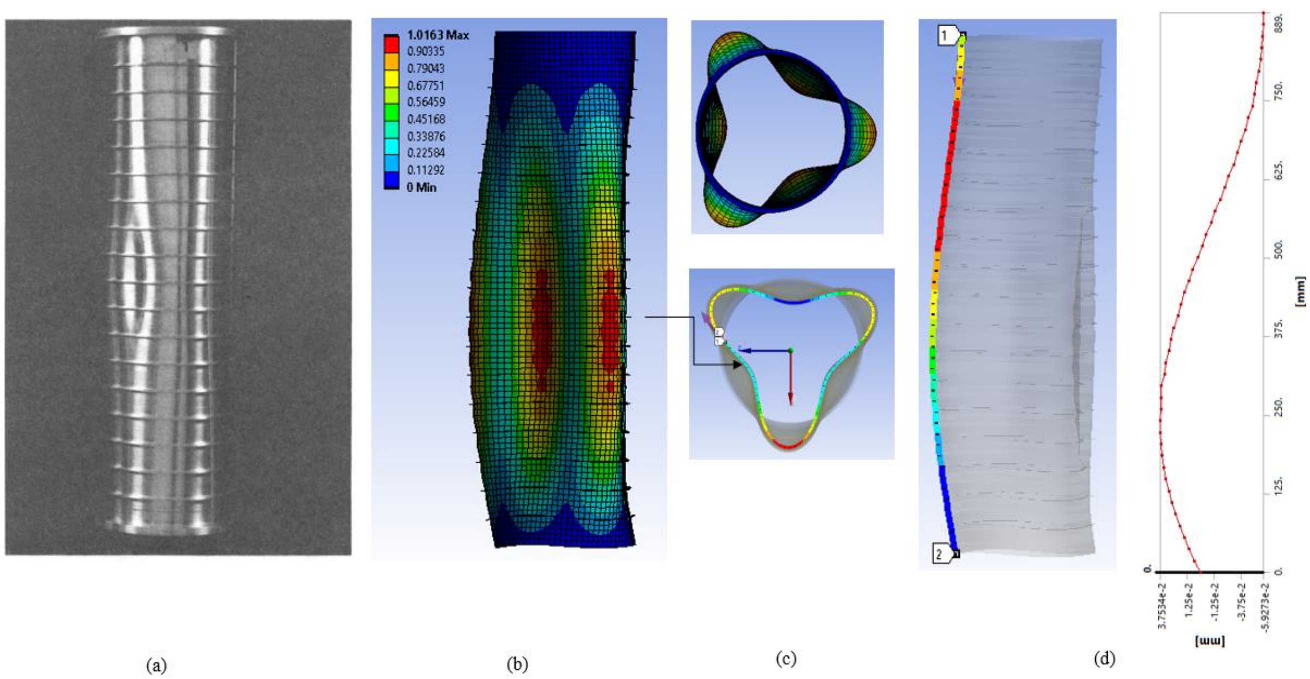

Figure 5-5. Specimen No. 1 at failure (a) Experimental (b) FE isometric view (c) FE top view (d) Longitudinal deflection along the given path

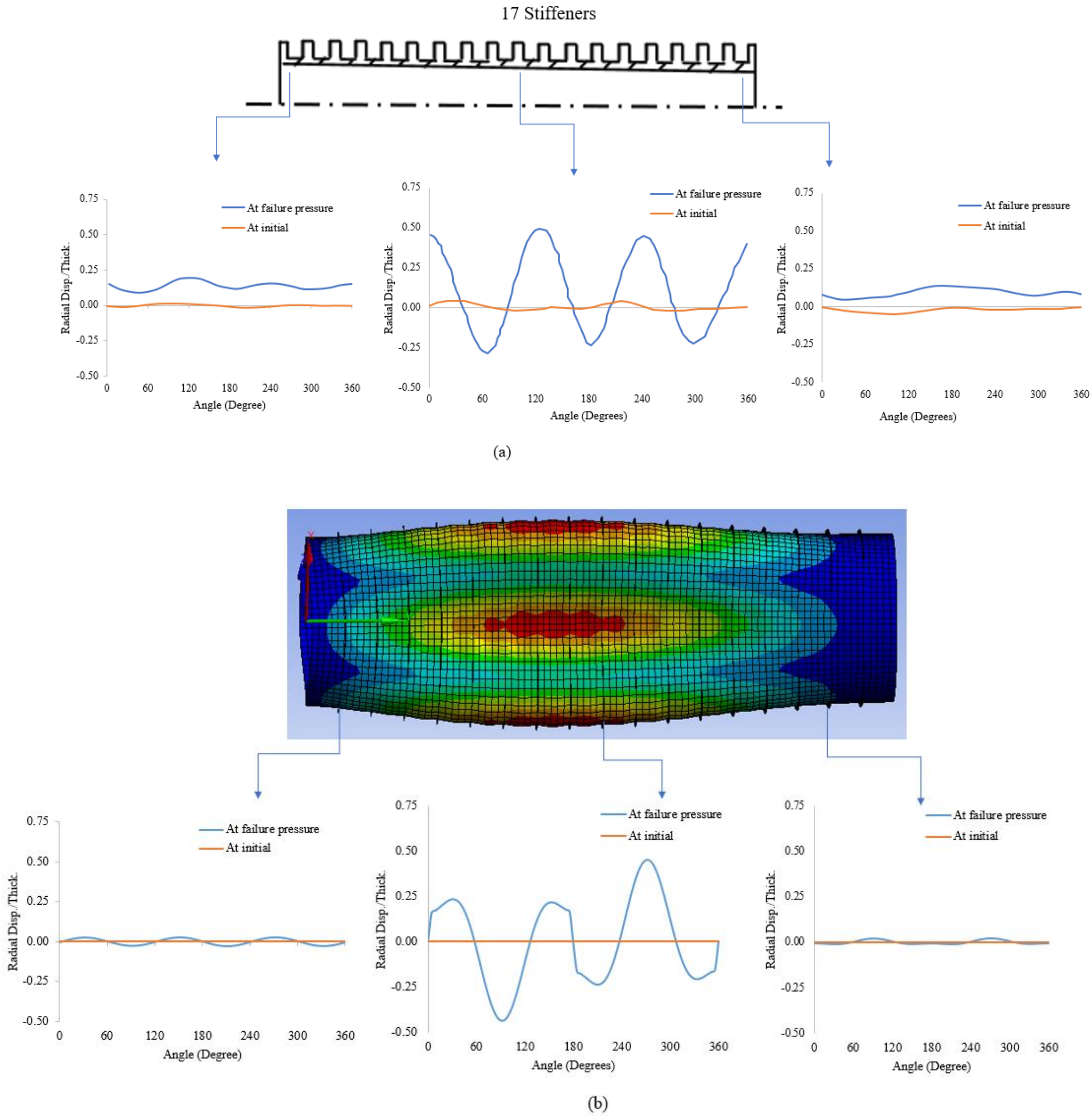

Figure 5-6. Circularity contours for specimen No. 1 (a) Contouring regenerated from experiments. (b) FE contouring

Specimen No. 3 and specimen No. 10 had 13 ring stiffeners that failed at 2.25 MPa buckling pressure with an overall flexural buckling mode consisting of three circumferential failure lobes as illustrated in Figure 5-7 similar to the experimental failure observation. The corresponding experimental value for specimen No. 3 was 2.96 MPa. The experimental buckling pressure for specimen No. 10 indicated a slightly higher value of 3.17 MPa compared to 2.96 MPa for specimen No. 3 due to the unequal imperfection conditions.

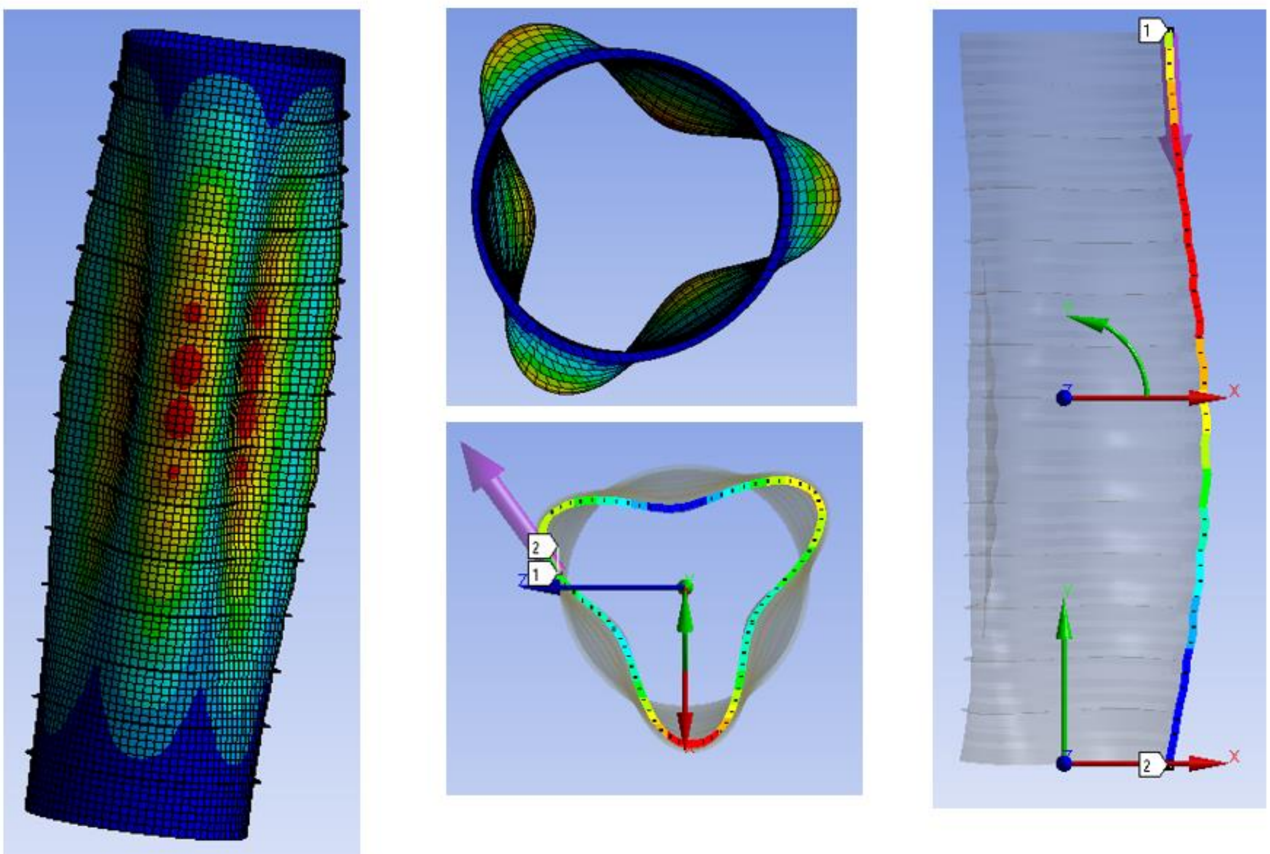

(a) (b) (c)

Figure 5-7. Specimen No. 3 at failure (a) FE isometric view (b) FE top view (c) Longitudinal deflection along the given path

Local shell buckling mode

Specimen No. 2 and specimen No. 9 had 3 stiffeners, failed in the local shell buckling mode at 1.45 MPa buckling pressure with six circumferential lobes confined in the bottom bay as shown in Figure 5-8. The radial deformation in other bays was not excessive as illustrated in the longitudinal deformation Figure 5-8(d) which indicates localized nature of shell buckling mode. Figure 5-8(a) illustrates the experimental failure shape with only one lobe; however, shell circularity contours for the bottom bay at failure indicated six circumferential lobes in experimental work as shown in Figure 5-9. The experimental buckling pressure for specimen No. 2 was 1.61 MPa compared to specimen No. 9 with 1.26 MPa, which might be due to the unequal imperfection conditions. The buckling pressure from linear FEA for the corresponding specimens is 1.45 MPa which falls between the two tests values.

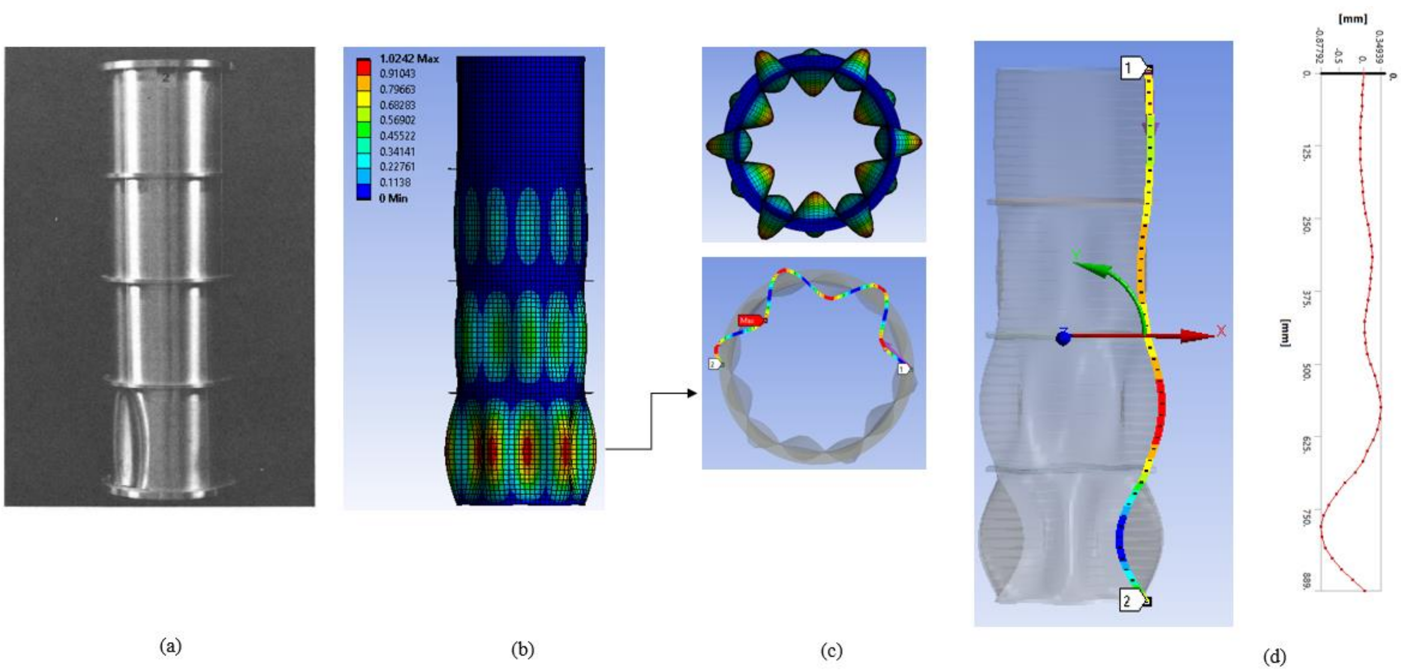

Figure 5-8. Specimen No. 2 at failure a) Experimental b) FE isometric view c) FE top view (d) Longitudinal deflection along the given path

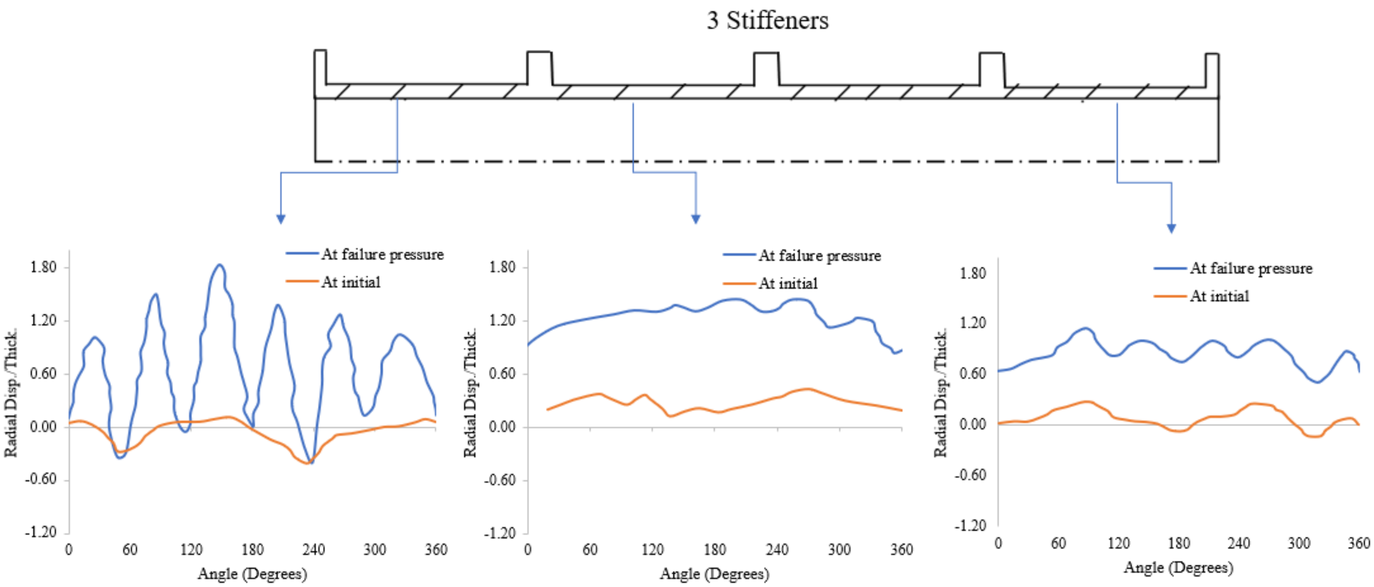

(a)

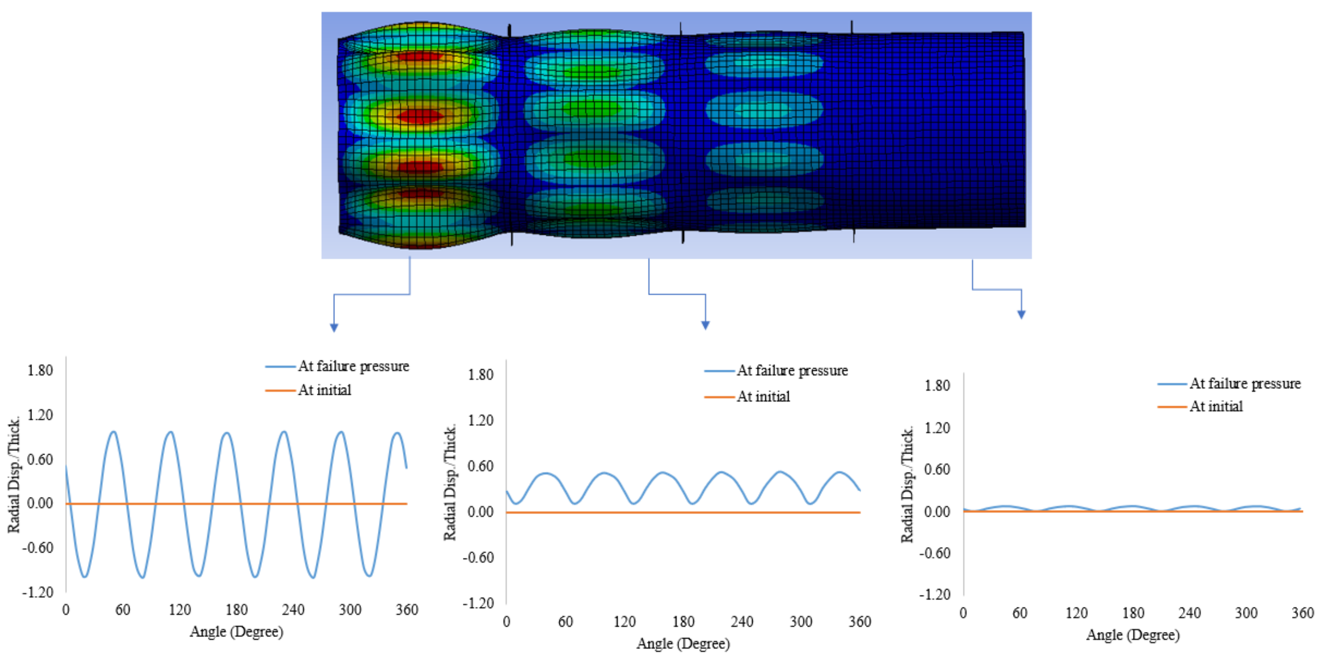

(b)

Figure 5-9. Circularity contours for specimen No. 2 (a) Contouring regenerated from experiments. (b) FE contouring

Specimen No. 4 had 5 ring stiffeners failure with the local shell failure mode, and seven circumferential lobes were observed at failure as shown in Figure 5-10, compared to the eight lobes observed in experiment. The FE linear buckling pressure is 2.18 MPa, compared to the experimental critical pressure of 2.36 MPa.

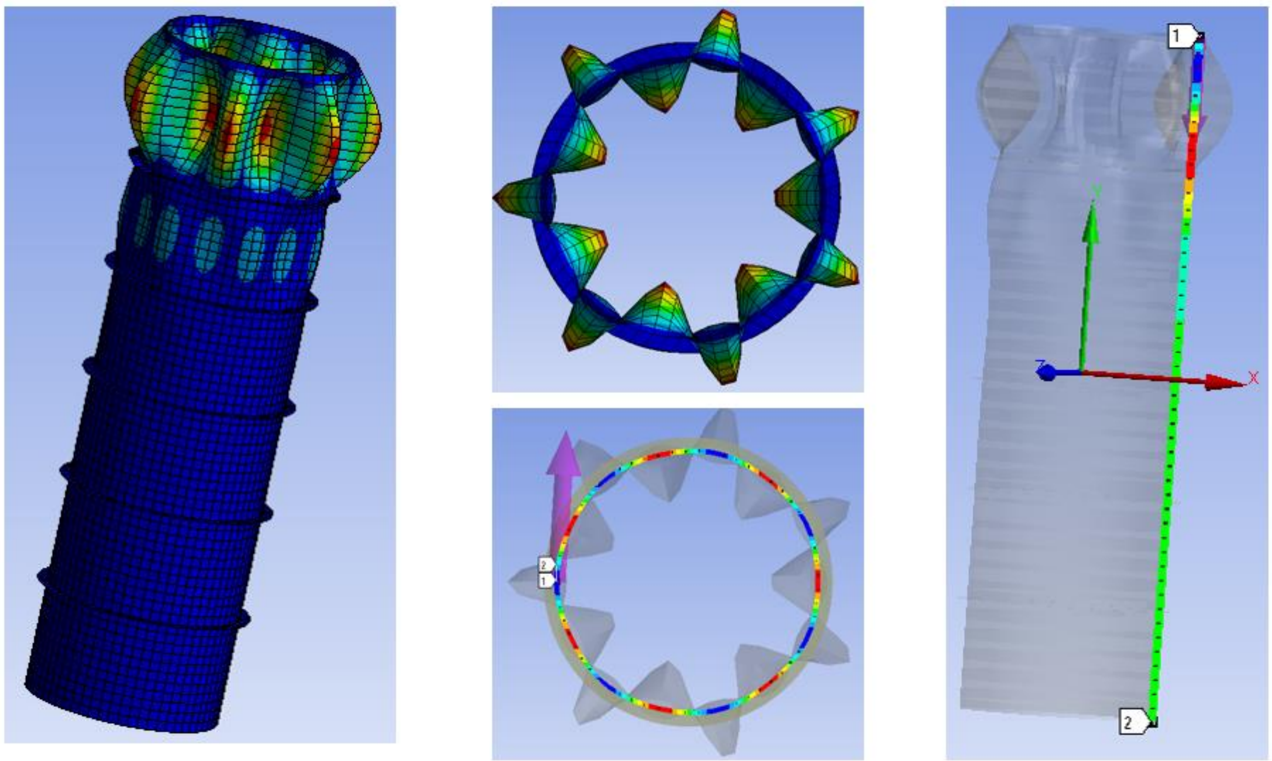

(a) (b) (c)

Figure 5-10. Specimen No. 4 at failure (a) FE isometric view (b) FE top view (c) Longitudinal deflection along the given path

Interactive buckling failure mode

Specimen No. 5 had 11 ring stiffeners that failed with interactive buckling mode mixed with local and overall flexural buckling. The dominant failure pattern was the overall flexural buckling mode; however, the local shell buckling mode influenced the final failure shape as proven by the experimental work. The failure occurred at 2.49 MPa with three lobes initiating from the middle bay as shown in Figure 5-11 compared to the corresponding experimental value of 3.28 MPa. The longitudinal deformation given in Figure 5-11(d) illustrates failure lobes confined between rings in multiple middle bays showed different failure nature compared to the specimen failed with overall flexural buckling mode which indicates interactive nature of the failure mode. Figure 5-12(a) illustrates the experimental failure shape with three circumferential lobes in the middle bays and seven minor lobes in the top bay; however, finite element shell circularity contours at middle and top bays represent three circumferential lobes as shown in Figure 5-12(b).

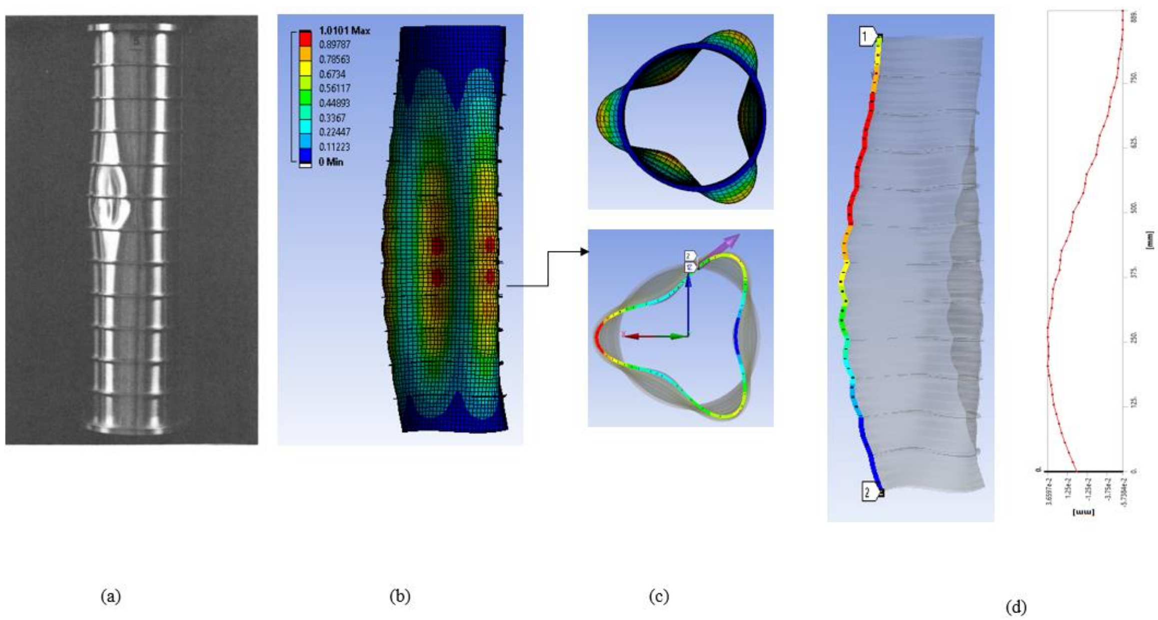

Figure 5-11. Specimen No. 5 after failure a) Experimental b) FE isometric view c) FE top view (d) Longitudinal deflection along the given path

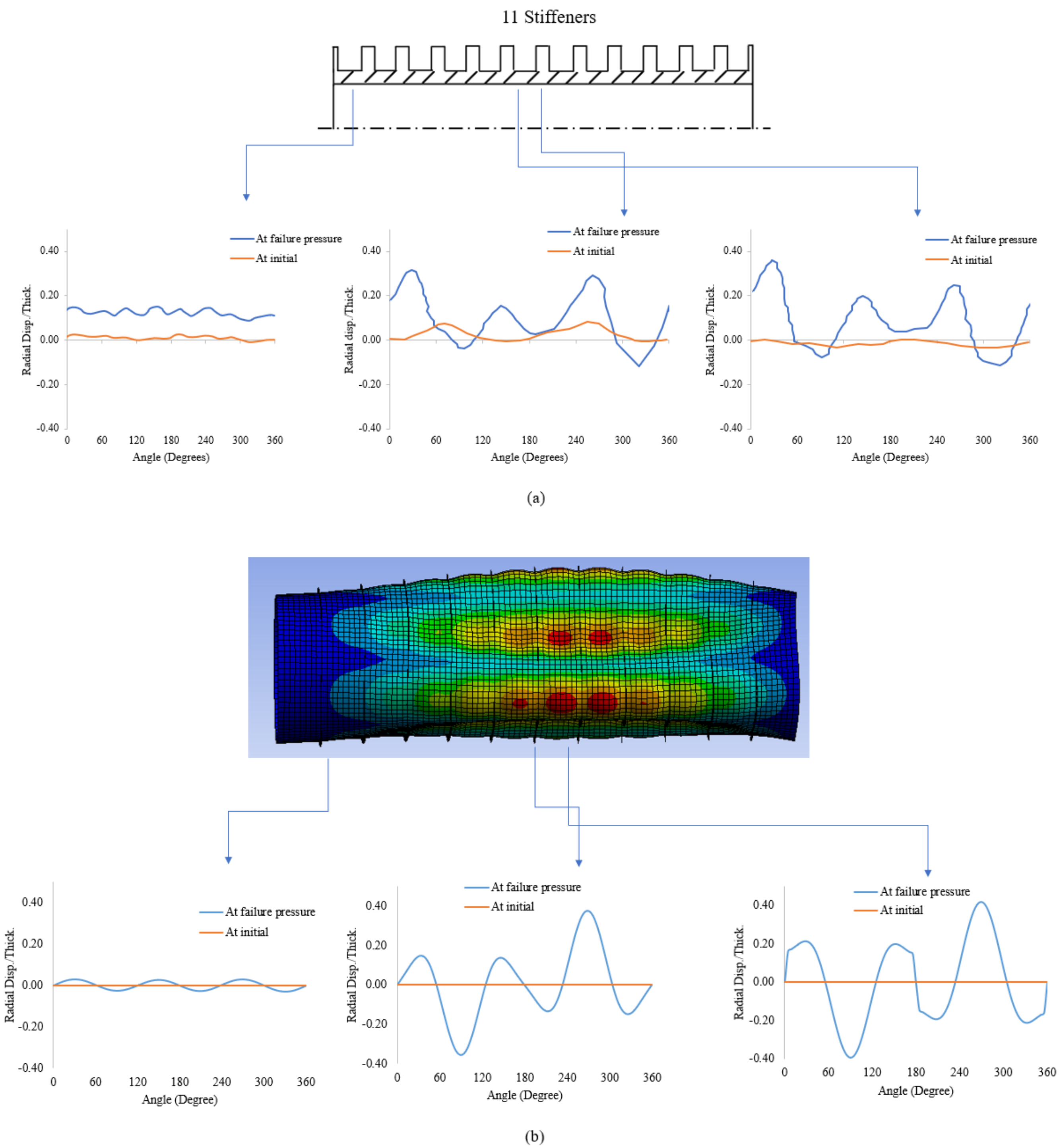

Figure 5-12. Circularity contours for specimen No. 5 (a) Contouring regenerated from experiments. (b) FE contouring

Specimen No. 8 with 9 stiffeners failed with interactive buckling mode mixed with local and overall flexural buckling. Three circumferential lobes initiating from the middle bay showed overall flexural buckling mode dominancy along with a several small deformations pattern confined between the rings which represent local shell buckling lobes. The FE linear buckling pressure is 2.63 MPa compared to the corresponding experimental value of 3.58 MPa.

Specimen No. 7 was similar to specimen No. 8 and had nine-ring stiffeners failed with interactive buckling mode at 2.63 MPa. Although overall flexural buckling mode dominant over local shell buckling mode as mentioned above and illustrated in Figure 5-13; however, the experimental results indicated primarily a local shell failure with eight lobes for specimen No. 7 compared to specimen No. 8, which might be due to the similar failure tendency for middle-range ring-stiffened cylinder specimens. The experimental buckling pressure for specimen No. 7 was 4.06 MPa compared to the 3.58 MPa for specimen No.8 obtained from the Southwell method. The Southwell method generally gave overestimated results; however, the experimental value for specimen No. 7 is remarkably high compared to the other experimental results for tested specimens, and it might be due to an accidental error during experimental work.

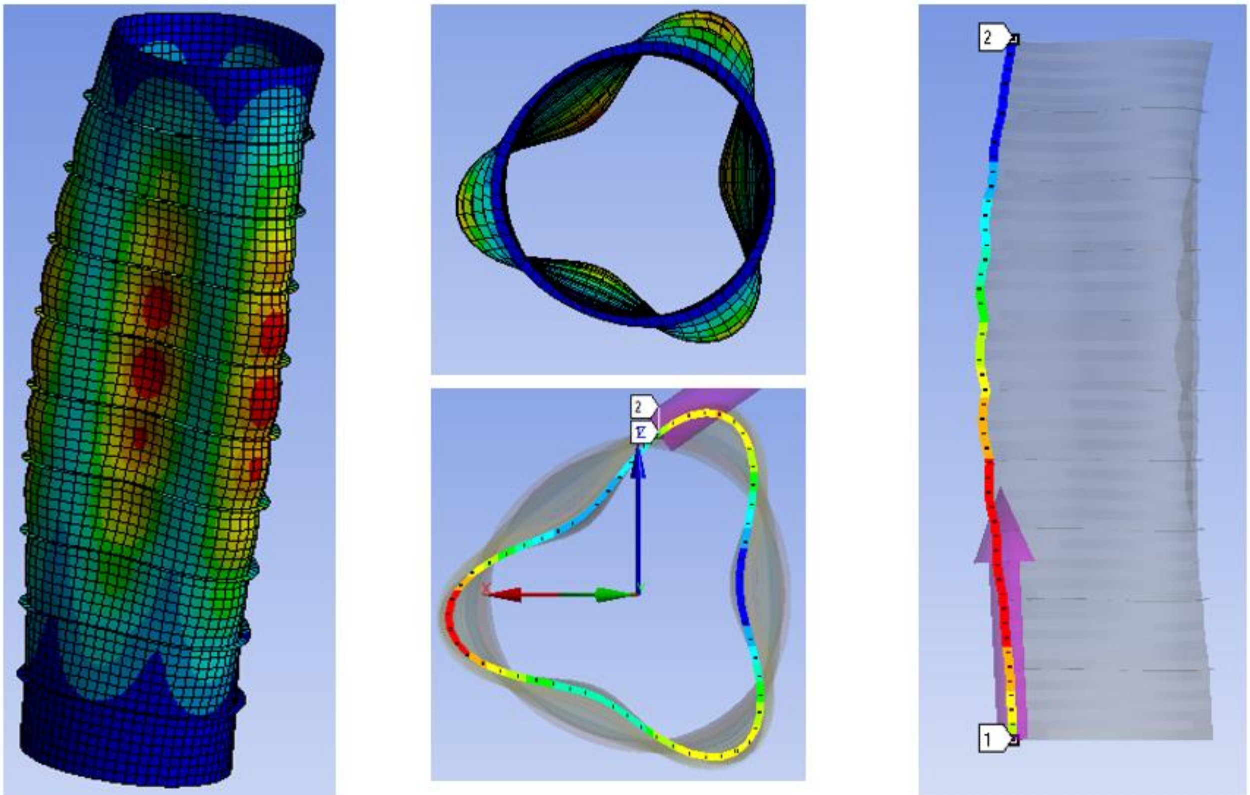

(a) (b) (c)

Figure 5-13. Specimen No. 7 at failure (a) FE isometric view (b) FE top view (c) Longitudinal deflection along the given path

Specimen No. 6 with 7 stiffeners also failed with interactive buckling mode. The six small lobes confined between the rings were observed numerically instead of eight lobes observed in experimental work at failure. Overall failure shape was influenced due to the excessive deformations observed in other bays and buildup of a three lobe which support the influence of overall flexural buckling mode as illustrated in Figure 5-14. The FE failure buckling pressure is 2.93 MPa compared to the experimental critical pressure of 3.60 MPa.

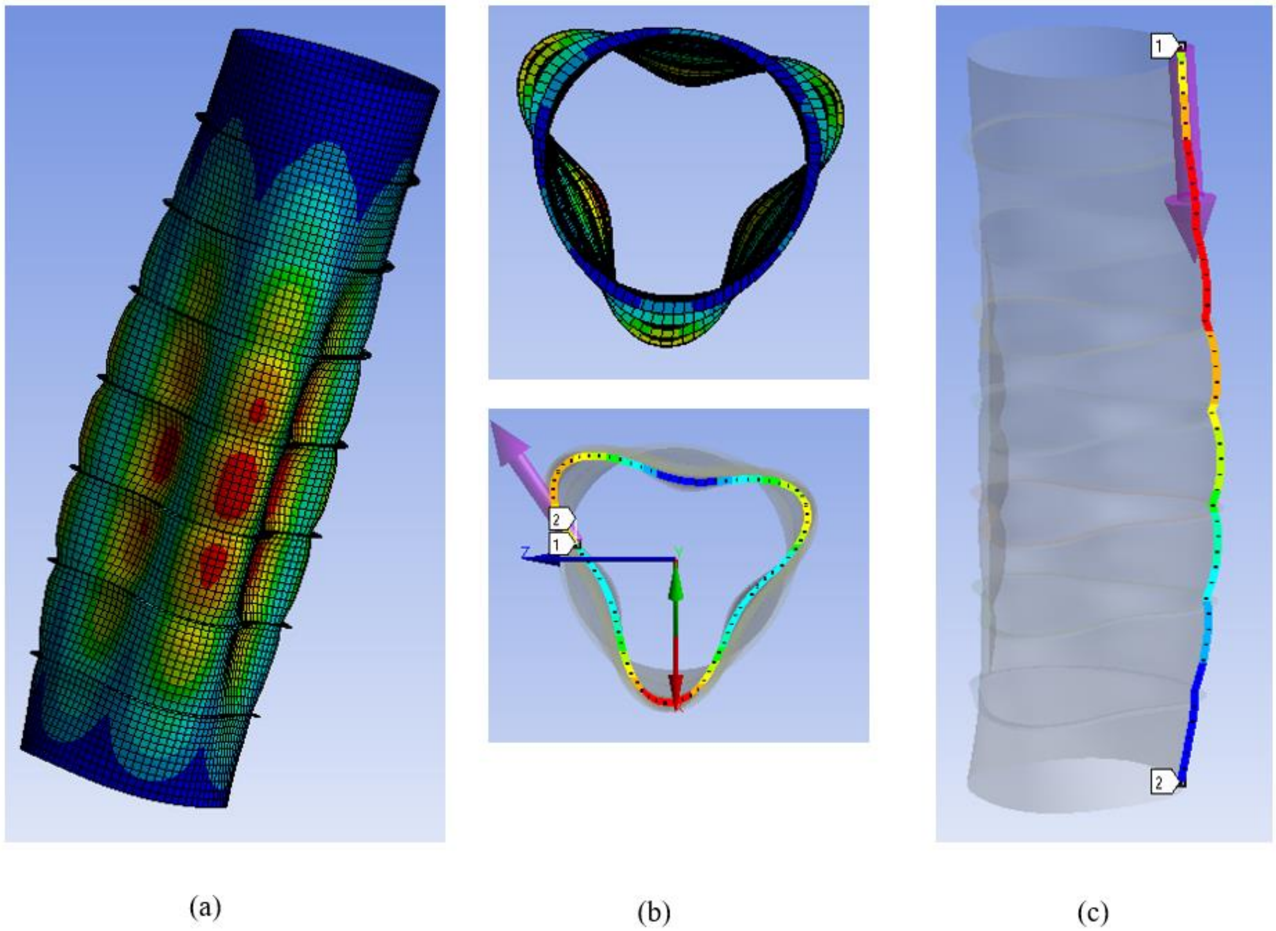

Figure 5-14. Specimen No. 6 at failure (a) FE isometric view (b) FE top view (c) Longitudinal deflection along the given path

5.3.4 Results Discussion

Specimens with lighter stiffeners failed with overall flexural failure mode while the specimens with stronger stiffeners failed with local shell buckling mode based on the dominant failure mode. The finite element buckling mode shapes for ring-stiffened cylindrical shells failed with overall flexural buckling modes similar to the failure pattern observed during the experiments. Numerical buckling pressures obtained from the linear analysis are lower than the corresponding experimental critical pressures; however, they compare well with the buckling pressure obtained from the Bryant and Kendrick equations. Although the Kendrick equation usually compares well with the experimental results for overall flexural buckling modes in literature [41]; however, it consistently underestimates the buckling pressure values similar to the Bryant equation and finite element results for the present studies.

For local shell buckling modes, numerical failure mode shapes were similar to the experimental failure pattern; however, the number of circumferential lobes obtained numerically for specimens No. 6 were six instead of eight observed during the experiment. Numerical buckling pressures obtained from the linear analysis and theoretical failure pressure obtained from the Greiner [33] were lower than the corresponding experimental results.

The difference between the experimental and numerical or theoretical buckling pressures is due to several reasons. Saleim and Roorda [16] used the Southwell technique to estimate the critical buckling pressure using experimental results obtained from the imperfect cylindrical shell. The Southwell technique was easy to implement but gave overestimated results. Additionally, higher experimental results than the numerical or theoretical results might be due to the stable symmetric post-buckling behavior. Saleim [42] performed non-linear post-buckling analysis for ring-stiffened cylinders and confirmed stable symmetric post-buckling behavior for both failure modes. The higher experimental pressure than the theoretical value was also observed in some other studies due to the stable symmetric post-buckling behavior for certain cylinders [32].

A plot between the number of stiffeners and critical buckling pressure calculated by all approaches is illustrated in Figure 5-15,Figure 5-16 and Figure 5-17. Figure 5-15 includes the overall flexural buckling mode with stiffeners ranging from 9 to 17. Results reveal that the critical buckling pressure decreases with the number of ring stiffeners increases since a larger number gives lighter stiffeners. Experimental critical buckling pressure gives higher results than others. Figure 5-16 represents the local shell buckling mode obtained from the smaller number of ring stiffeners ranging from 3 to 9. Critical buckling pressure is proportionally increased with the number of ring stiffeners. Figure 5-17 represents the overall buckling pressure results in comparison based on the number of ring stiffeners varying from 3 to 17. Failure mode types shifted from local shell buckling modes to the overall flexural buckling modes while increasing the number of ring stiffeners. The middle range ring stiffened cylinder specimens failed in one of the two possible modes and mostly flexural buckling for the present study; however, their failure pattern was influenced by the other mode, as proven by the experimental work.

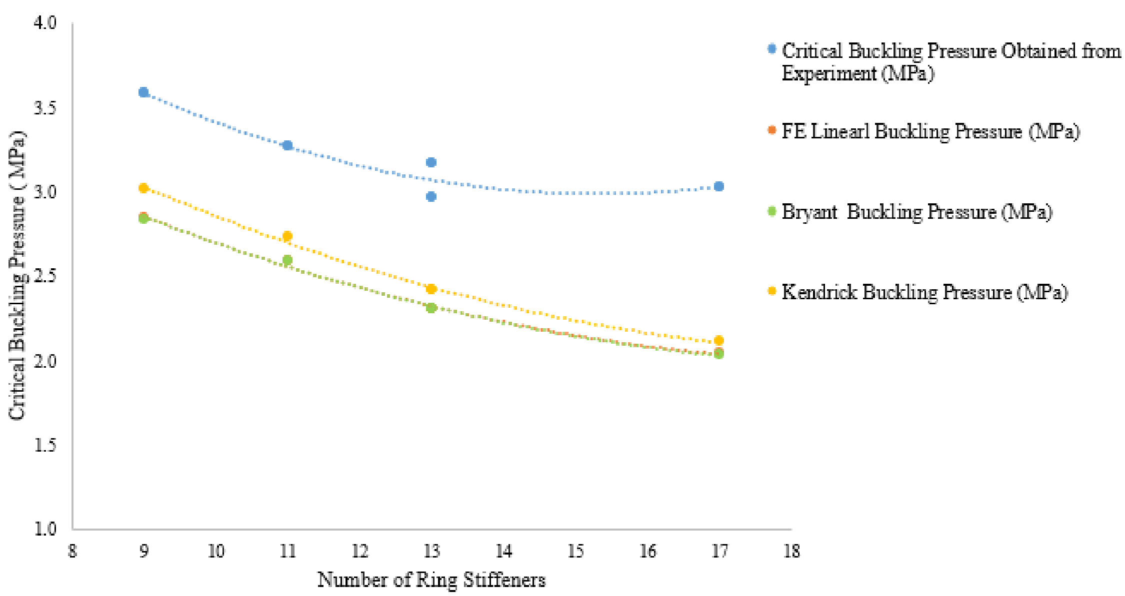

Figure 5-15. Buckling pressure results comparison: OFBM

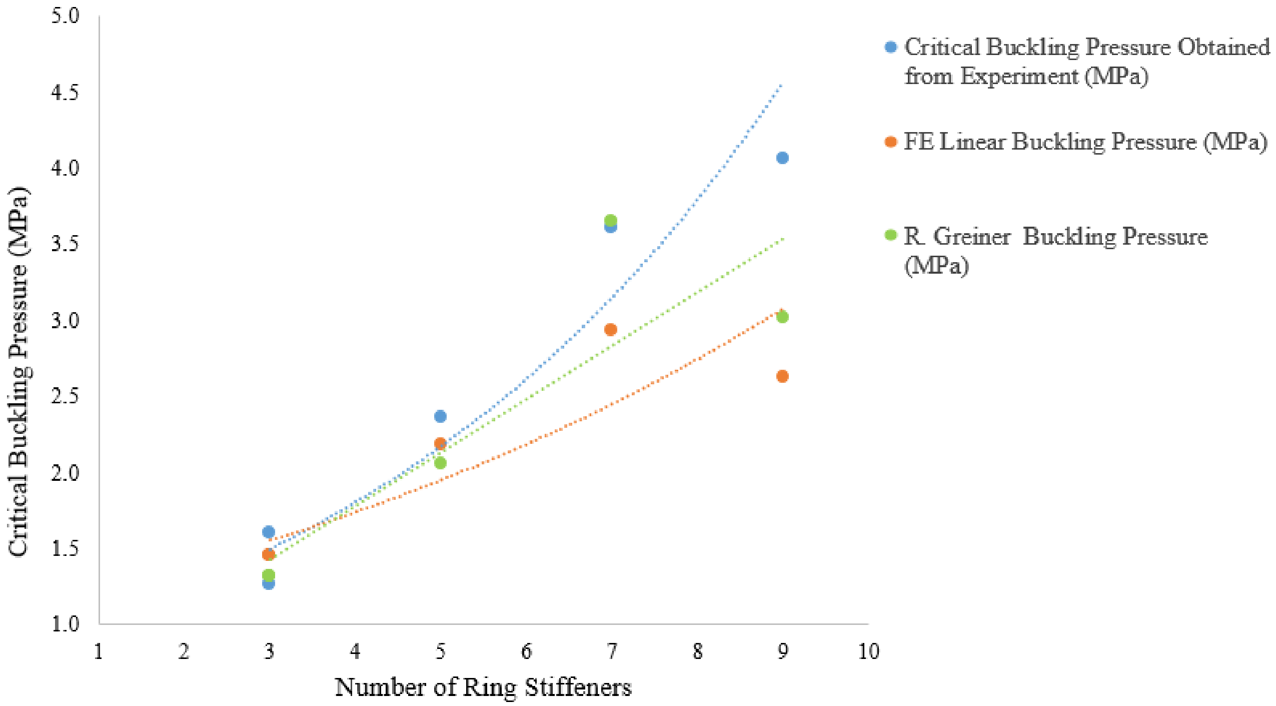

Figure 5-16. Buckling pressure results comparison: LSBM

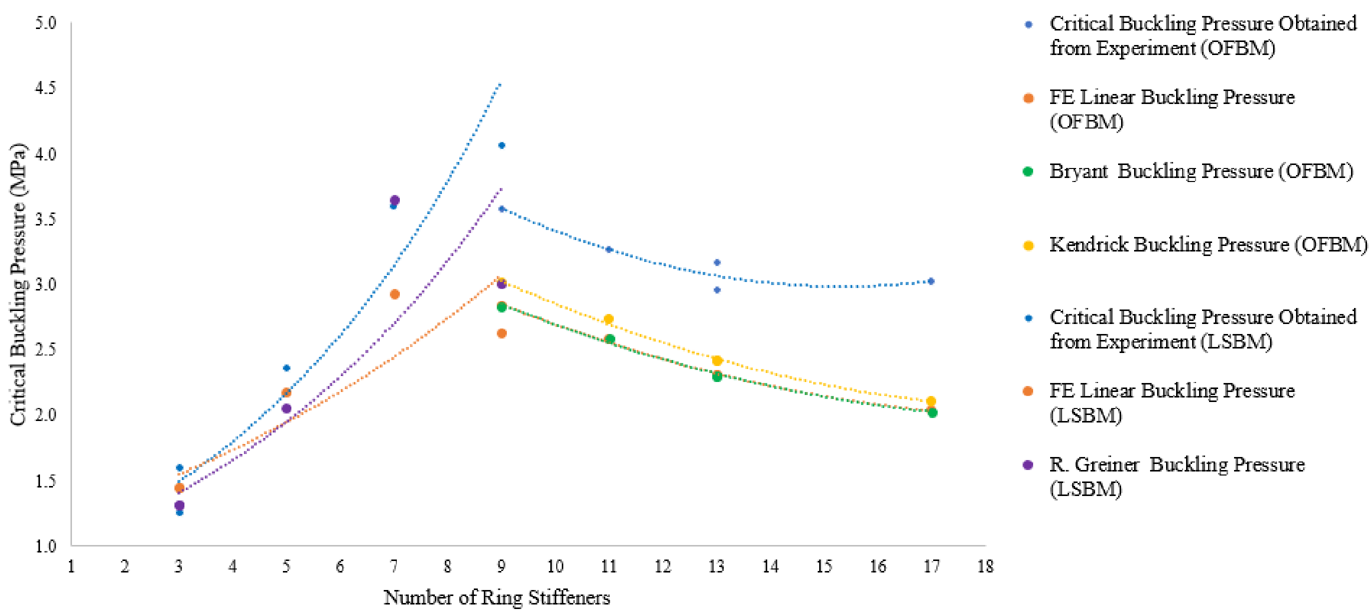

Figure 5-17. Overall buckling pressure results in comparison

5.4 Non-Linear Analysis

Nonlinear analysis was performed for all specimens. The mesh convergence study determined the optimum mesh size for all specimens based on the linear analysis, and the same mesh size was considered in the nonlinear analysis. Non-linear analysis was performed in two ways: non-linear analysis for perfect geometry and non-linear analysis for imperfect geometry based on eigenmode shapes obtained from the linear analysis.

5.5 Non-Linear Analysis (NLA) for Perfect Geometry

This technique is based on the non-linear static (Riks) analysis [43] using perfect geometry (PG) considering large deflection. All specimens were subjected to uniform external lateral pressure higher than the critical buckling pressure predicted from the linear analysis. A simply supported boundary condition was applied by constraining all nodes at the top and bottom edges for all cylinders; however, only axial displacement was allowed at the bottom edge. A ring-stiffened specimen No. 7 with 3 MPa external pressure about 10% higher than the linear buckling pressure predicted from the linear analysis and simply supported boundary condition is illustrated as an example in Figure 5-18a. The ultimate load in the FE modelling is subdivided into different load increments called load steps. These load steps are further subdivided into sub-steps [44]. For specimen No.7, external pressure is applied gradually considering 10 sec initial time increment but the value of "time" changes in the following load steps. The total substeps were 300, and the step end time was considered 3000 sec. The goal is to obtain critical pressure at the failure point. The failure occurred at 178 sub-steps at the time of 2645 sec. Therefore, the numerical failure pressure was 2.645 MPa compared to the corresponding experimental value of 2.941 MPa. The failure shape with the location of maximum nodal displacement for specimen No. 7 is illustrated in Figure 5-18b. The load-deformation curve at the location of maximum nodal displacement for specimen No. 7 is illustrated in Figure 5-19 as an example.

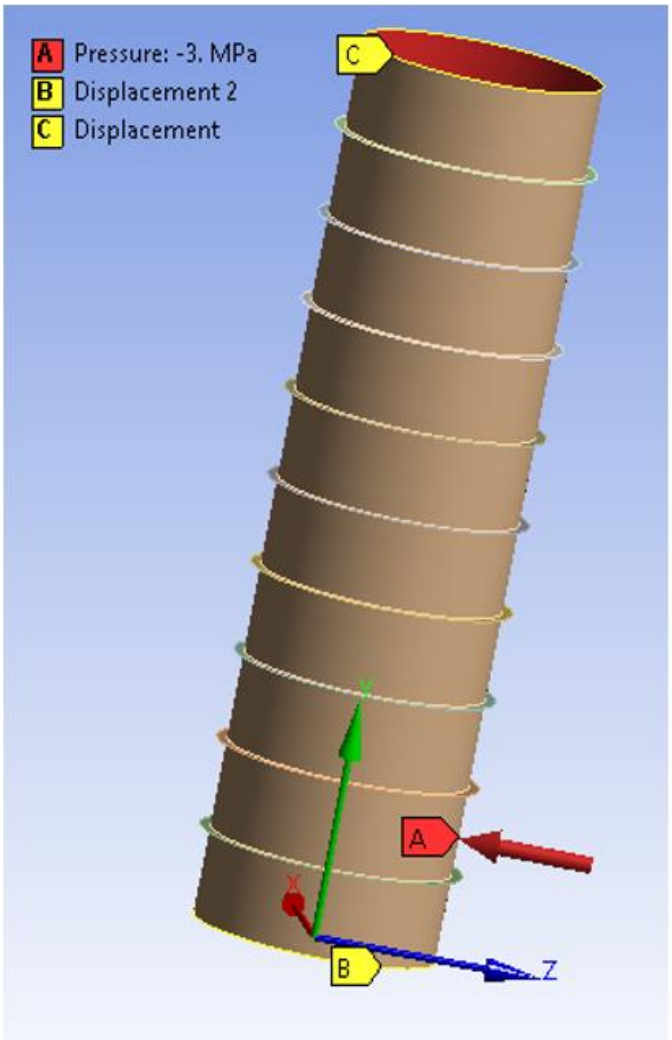

(a)

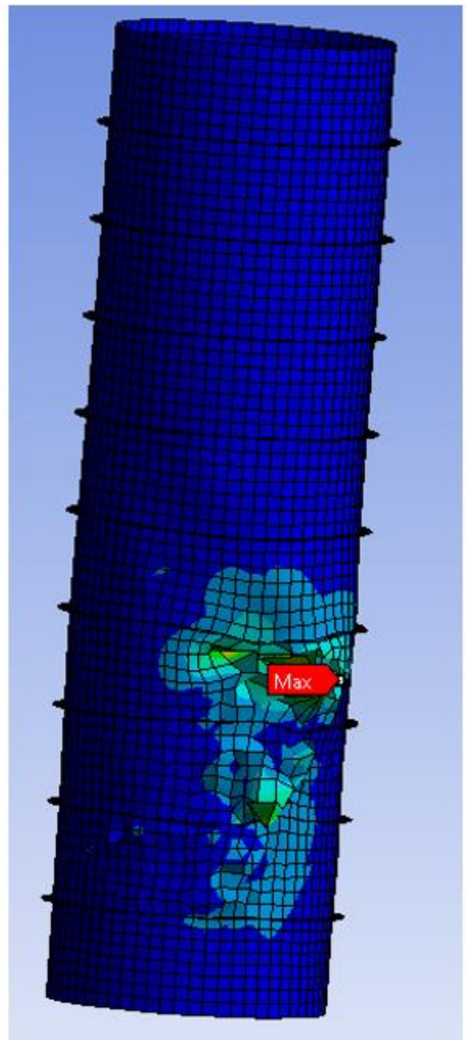

(b)

Figure 5-18. Non-Linear Analysis (NLA): (a) Specimen No. 7 geometry with loading and B.C (b) Failure shape with the location of maximum nodal displacement

The failure pressures obtained from the non-linear analysis by considering perfect geometries for all specimens are lesser than compared to the experimental buckling pressures as expected. The failure deformation pattern obtained from the non-linear analysis for some specimens was different from the buckling mode shape obtained from the experimental results since specimens with 9 or fewer number of stiffeners were crushed instead of buckling for a nonlinear perfect geometry as illustrated in Figure 5-20, Figure 5-21, Figure 5-22, and Figure 5-23. The crushing behaviour at failure for perfect geometries undergoing nonlinear analysis was also observed in the literature [45]. Experimental and FE non-linear failure result comparison for all specimens are illustrated in Table 5-7.

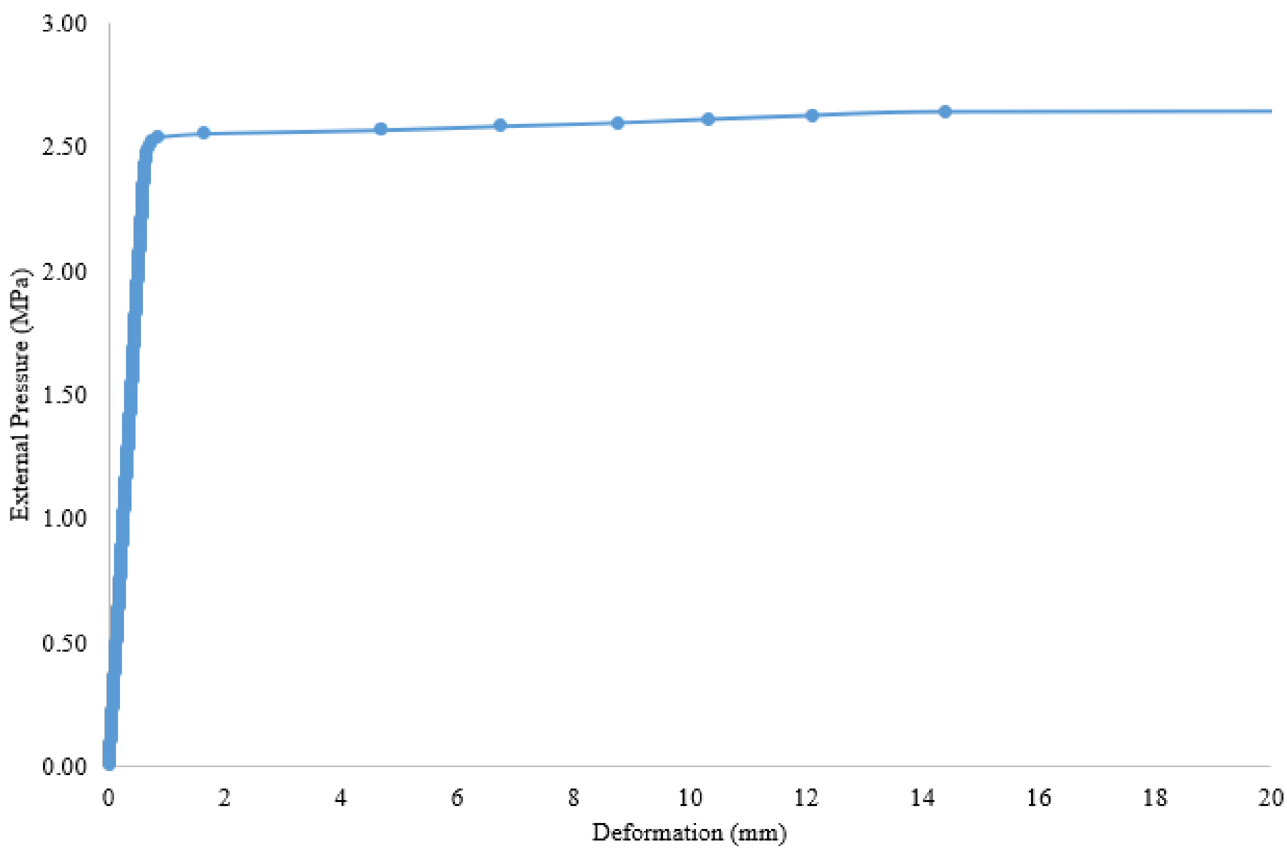

Figure 5-19. NLA: Load-deflection curve at the location of maximum nodal deflection for specimen No.7

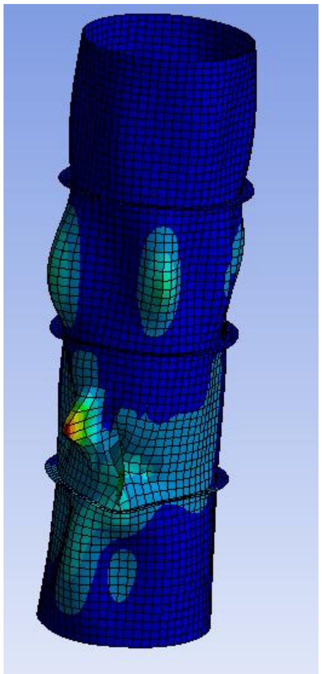

Figure 5-20. NLA: Specimen No. 2 crushing behaviour at failure

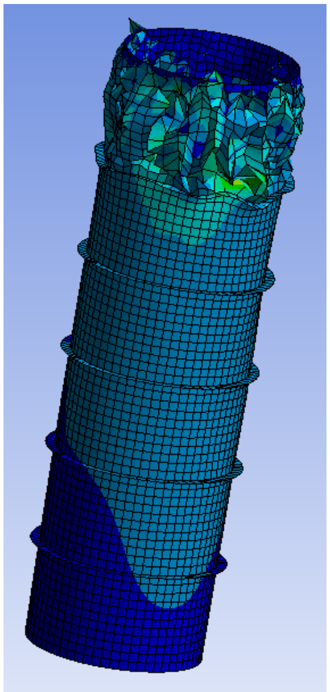

Figure 5-21. NLA: Specimen No. 4 crushing behaviour at failure

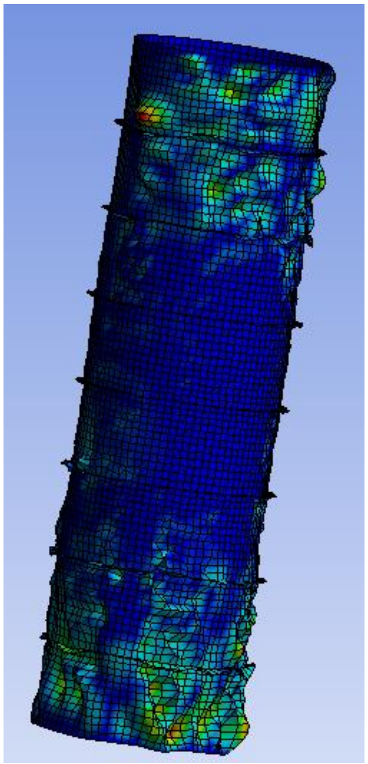

Figure 5-22 NLA: Specimen No. 6 crushing behaviour at failure

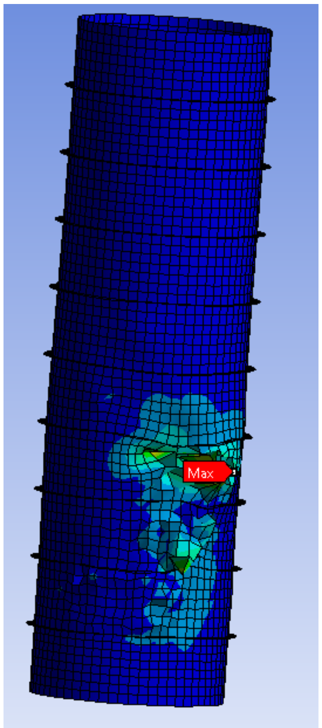

Figure 5-23 NLA: Specimen No. 7 crushing behaviour at failure

Table 5-7. Experimental Vs. FE non-linear failure pressure for perfect geometries

Sr. No.	No. of Stiffeners	Specimen No.	Experimental Failure Pressure (MPa)	FE NLA Failure Pressure for PG (MPa))	Experimental Failure Mode	FE NLA Failure Mode for PG (MPa)
1	3	2	1.57	1.44	LSBM	Crushed
2		9	1.06			
3	5	4	2.26	2.18	LSBM	Crushed
4	7	6	3.26	2.91	Interactive but dominant with LSBM	Crushed
5	9	7	2.94	2.65	Interactive but dominant with LSBM	Crushed
6		8	3.52		Interactive but dominant with OFBM	
7	11	5	3.19	2.52	Interactive but dominant with OFBM	Buckled with OFBM
8	13	3	2.83	2.29	OFBM	Buckled with OFBM
9		10	3.12			
10	17	1	3.03	2.10	OFBM	Buckled with OFBM

5.6 Non-Linear Analysis for Imperfect Geometry

Non-linear analysis considering imperfection is the most accurate approach for representing the true behaviour of actual imperfect structures if the measured imperfection is available. Imperfection sensitivity analysis based on the eigenmode shape can be employed if no appropriate imperfection data is available, as in this study [2]. Therefore, the eigenmode shape obtained from the linear analysis was considered an initial imperfection with renormalizing with the imperfection factor to get the buckling mode shape similar to the experimental results.

Imperfection Sensitivity Analysis

A uniformly pressurized cylindrical shell is less imperfection sensitive than the shell under compression due to the major difference in the buckling dimensions in the two cases [33]. Additionally, stiffened cylindrical shells exhibit less imperfection sensitivity than the equal mass unstiffened cylinders [2]. Therefore, an imperfection sensitivity analysis was performed to determine the lowest imperfection value but large enough to get the buckling mode shape similar to the experimental results. The initial imperfection shape is consistent with the first eigenmode shape obtained from the linear buckling analysis. The eigenmode shape was renormalized using an imperfection factor of 0.5, 1.0 ,5, 10, and 50 % for the present study. The failure mode shapes considering different imperfection factors for specimen No. 7 are illustrated in Figure 5-24 as an example. The results revealed that the 5% imperfection was the lowest value for specimens with 9 or lesser number of stiffeners, giving the failure mode shape similar to specimens' experimental buckling shape; however, for specimens with larger number of stiffeners gave similar failure shape even for imperfection lessor than 5%. For specimen No. 7, analysis does not converge at a lower sub step at the time of 2585 sec (2.59 MPa) compared to the experimental failure pressure. Therefore, the numerical failure pressure was 2.59 MPa compared to the corresponding nonlinear value of 2.65 MPa for perfect geometry and the experimental value of 2.94 MPa. The load-deflection curve at the location of maximum nodal deflection for specimen No. 7 represents the effect of different geometric imperfections on the failure pressure, as illustrated in Figure 5-25. Experimental and non-linear analysis results in comparison for all imperfect specimens with 5 % imperfection are illustrated in Table 5-8.

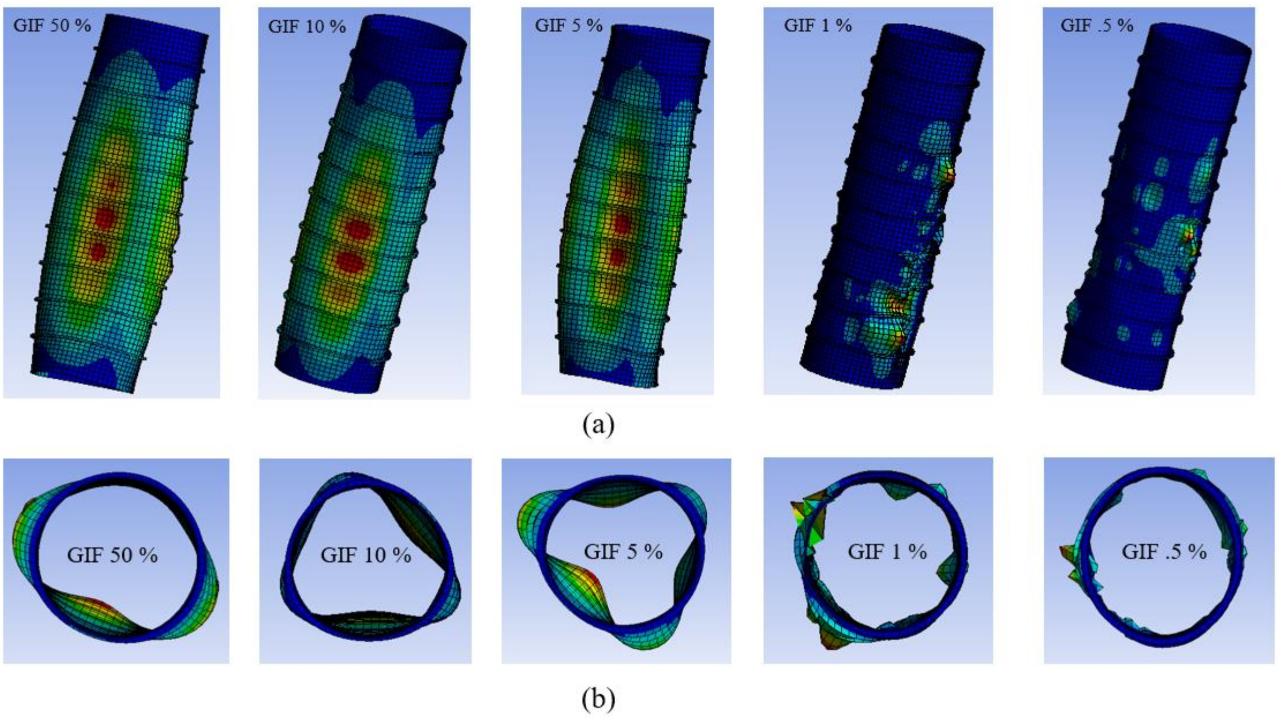

Figure 5-24. Specimen No. 7 mode shapes at different geometric imperfections (GIF) a) FE isometric view b) FE top view

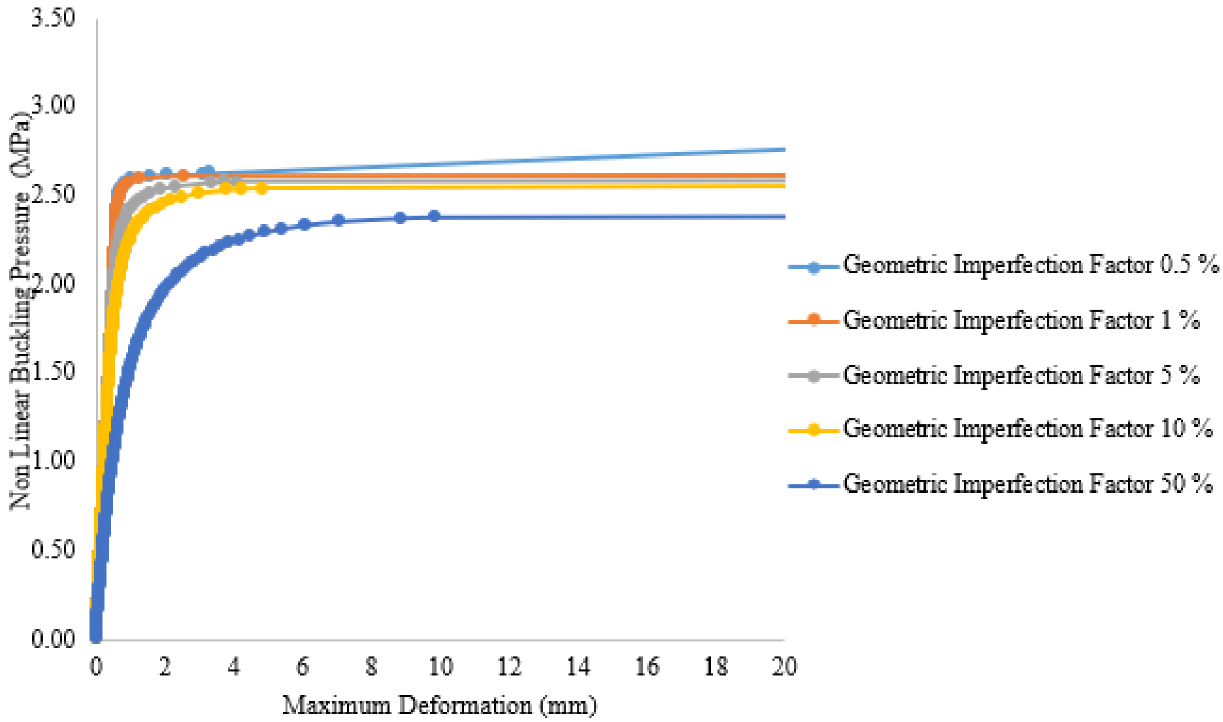

Figure 5-25. Effect of various GIF on the non-linear failure pressure for specimen No. 7

Table 5-8. Experimental Vs. FE NL failure pressure for all specimens (imperfect geometry)

Sr. No.	Number of Stiffeners	Specimen No.	Experimental Failure Pressure (MPa)	FE NLA Failure Pressure for Imperfect Geometry with 5 % GIF (MPa)
1	3	2	1.57	1.38
2		9	1.06	
3	5	4	2.26	2.16
4	7	6	3.26	2.87
5	9	7	2.94	2.59
6		8	3.52	
7	11	5	3.19	2.49
8	13	3	2.83	2.28
9		10	3.12	
10	17	1	3.03	2.08

5.7 Results Discussion

A comparison between the experimental failure pressure and numerical failure pressure obtained from the non-linear analysis for perfect and imperfect geometries is summarized in Table 5-9 and Table 5-10 for both types of failure. For local shell buckling mode, a comparison of the results revealed that the difference between the experimental and finite element non-linear failure pressure varies from a minimum of 3.33 % to a maximum of about 10.82 % for perfect geometries, while a minimum of 4.21 % to a maximum of about 12.04 % for imperfect geometries with 5 % imperfection. For overall shell buckling mode, this difference was a minimum of 20.98 % to a maximum of 30.72 % for perfect geometries and a minimum of 21.92 % to a maximum of 31.38 % for imperfect geometries with 5 % imperfection. It was also observed that some specimens were crushed instead of buckled at failure for non-linear perfect geometries. For nonlinear analysis of imperfect geometries, results revealed that the 5 % imperfection was the lowest value for most of the specimens, giving the failure mode shape similar to the experimental buckling shape. Results indicate that the buckling mode shape-shifted from the local shell buckling mode to the overall flexural buckling mode while increasing the number of stiffeners, similar to the linear analysis as well as experimental work.

Table 5-9. Experimental Vs. FE non-linear buckling pressure for LSBM

Specimen No.	Number of Stiffeners	Experimental Buckling Pressure (MPa)	FE NLA Failure Pressure for PG (MPa)	FE NLA Failure Pressure for Imperfect Geometry with 5 % GIF (MPa)	Percentage Difference between Exp and FE NLA (Perfect)	Percentage Difference between Exp and FE NLA (Imperfect)
2 & 9	3	1.32*	1.44	1.38	9.42	4.86
4	5	2.26	2.18	2.16	3.33	4.21
6	7	3.26	2.91	2.87	10.82	12.04
7	9	2.94	2.65	2.59	9.89	11.93

1.32* is an average value for specimen No. 2 and 9

Table 5-10. Experimental Vs. FE non-linear buckling pressure for OFBM

Specimen No.	Number of Stiffeners	Experimental Buckling Pressure (MPa)	FE NLA Failure Pressure for PG (MPa)	FE NLA Failure Pressure for Imperfect Geometry with 5 % GIF (MPa)	Percentage Difference between Exp and FE NLA (Perfect)	Percentage Difference between Exp and FE NLA (Imperfect)
8	9	3.52	2.65	2.59	24.67	26.38
5	11	3.19	2.52	2.49	20.98	21.92
3 & 10	13	2.97*	2.29	2.28	22.90	23.23
1	17	3.03	2.10	2.08	30.72	31.38

2.97* is an average value for specimen No. 3 and 10

5.8 Effect of Constant Stiffener Height on the Buckling Strength: A Parametric Study

An average stiffener height of 11 mm for all specimens was considered for further parametric studies without changing the overall stiffener cross-sectional area. The stiffener thicknesses vary from 2.38 mm to 13.56 mm by keeping the stiffener height constant, but the overall cylindrical weight remained the same for all specimens. Table 5-11 illustrates the effect of constant stiffener height by using linear analysis. Results indicate that specimen with 7 and a larger number of stiffeners failed in the overall flexural buckling mode, and the other with 5 and a lesser number of stiffeners failed in the local shell buckling mode. The linear buckling strength remarkably improved by keeping a constant stiffener height compared to the FE linear buckling pressure for specimen dimensions obtained from experiments. Although, the buckling strength improvement for local shell buckling mode are not significant; however, strength improvement goes to the maximum of about 56.37 % for overall shell buckling mode. Furthermore, it was observed that the number of circumferential failure lobes decreases for both types of failure as illustrated in Table 5-11. The effect of constant stiffener height is also investigated by using nonlinear analysis for all specimens with 5% imperfections. Table 5-12 illustrates the improvement in the nonlinear buckling strength by keeping a constant stiffener height compared to the FE nonlinear failure pressure for specimen dimensions obtained from experiments with 5% imperfections.

Table 5-11. Effect of constant stiffener height on the linear buckling strength

Serial No.	Specimen No.	Number of Stiffeners	FE Linear Buckling Pressure (MPa)	FE Critical Buckling Pressure with constant h_s (MPa)	% age improvement in buckling strength
1	2 & 9	3	1.45 (6)	1.46 (6)	0.69
2	4	5	2.18 (8)	2.18 (7)	0.46
3	6	7	2.93 (7)	2.95 (3)	0.68
4	7	9	2.63 (3)	2.99 (3)	13.69
5	5	11	2.49 (3)	3.05 (2)	22.49
6	3 & 10	13	2.25 (3)	3.07 (2)	36.44
7	1	17	2.04 (3)	3.19 (2)	56.37

Table 5-12. Effect of constant stiffener height on the non-linear failure strength

Serial No.	Specimen No.	Number of Stiffeners	FE NLA Buckling Pressure (MPa)	FE NLA Buckling Pressure with constant h_s (MPa)	% age improvement in buckling strength
1	2 & 9	3	1.38	1.43	3.62
2	4	5	2.16	2.19	1.39
3	6	7	2.87	2.88	0.35
4	7	9	2.59	2.93	13.13
5	5	11	2.49	3.01	20.88
6	3 & 10	13	2.28	3.05	33.77
7	1	17	2.08	3.11	49.52

6 Summary and Future Work

Based on the extensive study of this thesis, the buckling behaviors of the metallic cylindrical tanks are investigated. The extensive parameters related to the buckling behavior of metallic cylindrical tanks are analyzed. The extensive parameters in this thesis are (1) A verification of the overall performance and quality of the numerical modeling approach, and computational analysis to calculate the linear buckling behaviour of empty cylindrical shells with different *H/D* and *D/t* ratios using ANSYS workbench 2021, (2) To investigate the effect of *R/t* and *H/R* ratios and real imperfections on the buckling strength of cylindrical tank specimens subjected to external pressure using the finite element technique, (3) To numerically investigate the effect of external ring-stiffeners size and spacing on the failure modes and buckling pressure of stiffened cylinders subjected to the uniform external lateral pressure, (4) To perform imperfection sensitivity analysis based on the eigenmode shape obtained from the linear analysis, (5) To numerically investigate the effect of constant stiffener height on linear and nonlinear buckling strength for further parametric studies.

The accuracy of FEM is ensured with the existing experiment and well-known theoretical equations. The following noteworthy points are summarized within the scope of this thesis:

For steel made cylindrical specimens subjected to the compressive load; The FEA models accurately predict static critical buckling stress which is mainly depends on the *D/t* ratio. The solution of the buckling analysis provides multiple buckling mode shapes and critically buckling load values. Those mode shapes (eigenvectors) can indicate the expected buckling modes during the nonlinear analysis.

For steel made cylindrical specimens subjected to external pressure; varying *R/t* and *H/R* ratios strongly influence the critical buckling pressure. The buckling pressure remarkably increases with the decrease of both *R/t* and *H/R* ratios; however, the effect of the *R/t* ratio is more dominant than the *H/R* ratio. The Results revealed that the geometric imperfections have little influence on the overall buckling capacity, especially for tanks with large *H/R* ratios and smaller *R/t* ratios. Numerical results show good agreement with experimental and theoretical results; however, FEA gave higher results, especially for cylinders with smaller *R/t* ratios might be due to neglecting imperfections that are probably created in the construction process.

For Aluminium made thin-walled stiffened cylindrical specimens subjected to the external pressure; the following noteworthy points were concluded based on the finite element linear, non-linear analysis, and parametric studies;

- The FE linear analysis indicates mainly two types of failure modes i.e. overall flexural buckling mode (OFBM) and local shell buckling mode (LSBM). Failure mode type shifted from local shell buckling mode to the overall flexural buckling mode while increasing the number of ring stiffeners. The middle range ring stiffened cylinder specimens failed in one of the two possible modes and mostly flexural buckling for the present study; however, their failure pattern was influenced by the other mode, as proven by the experimental work.
- The specimens with 9 and a larger number of stiffeners with lower strength failed in the overall flexural buckling mode (OFBM), and the other with 7 and a lesser number of stiffeners with higher strength failed in the local shell buckling mode (LSBM). The failure mode shapes and number of circumferential lobes at failure for all specimens obtained from the linear analysis closely matched the experimental failure pattern.

- The numerical buckling pressures obtained from the linear analysis were lower than the corresponding experimental critical pressures; however, they compare well with the buckling pressure obtained from the theoretical equations.
- The buckling pressures obtained from the FE non-linear analysis with perfect geometries are compared lessor to the experimental results. Moreover, specimens having 9 or lessor number of stiffeners were crushed instead of buckling at failure.
- For nonlinear analysis of imperfect geometries based on the eigenmode shape, results revealed that the 5 % imperfection was the lowest value for most of the specimens, giving the failure mode shape similar to the experimental buckling shape. The local shell buckling pressures obtained from the nonlinear analysis of imperfect geometries with 5 % imperfection were closer to the corresponding experimental buckling pressures compared to the buckling pressure for the specimens that failed with an overall flexural buckling mode shape.
- Parametric study reveals that both linear and nonlinear buckling strength remarkably improved by keeping a constant stiffener height compared to the FE buckling strength for specimen dimensions obtained from experiments especially for specimens failed with overall flexural buckling mode.
- The experimental, theoretical, and finite element (FE) results indicate that the ring stiffener's optimum size and spacing can improve the stiffened cylinder buckling strength since critical buckling pressure and failure mode shape were influenced by the ring stiffener's size and spacing.

Further parametric study will be conducted to investigate the impact of the radius-to-thickness ratio, length-to-radius ratio, boundary conditions, stiffener geometry and distance of stiffeners on the buckling response in more detail. The expected results will provide additional insight of the stiffened thin wall cylinders behavior and can guide the applications of thin shell structures with stiffeners in practice.

Study will continue to investigate the seismic effects on the buckling behavior of stiffened thin-walled cylinders as well and following are the key objectives which will be covered in future.

- To study the dynamic behavior of aboveground thin-walled stiffened cylinders under earthquake records to assess the earthquake signature and further assessment of seismic performance of stiffened tanks.
- Assessment of the effect/influence of imperfections and boundary conditions on the seismic behavior of thin-walled stiffened cylinders.
- Assessment of the Hydrostatic pressure, hoop stresses, axial compressive stresses w.r.t some important perimeters under worldwide well-known earthquake records
- Propose seismic design equations to investigate the seismic response of the liquid-filled thin-walled stiffened cylinders.

7 References

[1] H. Pasternak, Z. Li, and A. Jäger-Cañás, "Investigation of the buckling behaviour of ring-stiffened cylindrical shells under axial pressure," *ce/papers*, vol. 4, no. 2–4, pp. 2092–2097, 2021.

[2] M. W. Hilburger, "Buckling of Thin-Walled Circular Cylinders," 2020.

[3] W. Roopkumdee, "Seismic Response Of Liquid-Filled Thin-Walled Steel Cylindrical Tanks," 2021.

[4] T. V Galambos, *Guide to stability design criteria for metal structures*. John Wiley & Sons, 1998.

[5] S. Kendrick, "The buckling under external pressure of circular cylindrical shells with evenly spaced, equal strength, circular ring frames. Part II," Naval Construction Research Establishment, Dunfermline, Fife., Scotland …, 1953.

[6] W. A. Nash, "Buckling of multiple-bay ring-reinforced cylindrical shells subject to hydrostatic pressure," 1953.

[7] G. D. Galletly, R. C. Slankard, and E. Wenk Jr, "General instability of ring-stiffened cylindrical shells subject to external hydrostatic pressure—A comparison of theory and experiment," 1958.

[8] A. R. Bryant, "Hydrostatic pressure buckling of a ring-stiffened tube," *Nav. Constr. Res. Rep.*, 1954.

[9] B. Standard, "BS 5500, Specification for Unfired Fusion Welded Pressure Vessels." British Standards Publishing Limited, London, 1997.

[10] R. D. Ziemian, *Guide to stability design criteria for metal structures*. John Wiley & Sons, 2010.

[11] T. Weller and J. Singer, "Experimental studies on the buckling under axial compression of integrally stringer-stiffened circular cylindrical shells," 1977.

[12] C. D. Miller, "Buckling of axially compressed cylinders," *J. Struct. Div.*, vol. 103, no. 3, pp. 695–721, 1977.

[13] P. J. Dowling, J. E. Harding, N. Agelidis, and W. Fahy, "Buckling of orthogonally stiffened cylindrical shells used in offshore engineering," in *Buckling of shells*, Springer, 1982, pp. 239–273.

[14] A. Walker, A. Andronicou, and S. Sridharan, "Experimental investigation of the buckling of stiffened shells using small scale models," *Buckling Shells off-shore Struct. Granada London al*, pp. 45–71, 1982.

[15] A. C. Walker, Y. Segal, and S. McCall, "The buckling of thin-walled ring-stiffened steel shells," in *Buckling of shells*, Springer, 1982, pp. 275–304.

[16] S. S. Seleim and J. Roorda, "Buckling behaviour of ring-stiffned cylinders; experimental study," *Thin-walled Struct.*, vol. 4, no. 3, pp. 203–222, 1986.

[17] J. Tian, C. M. Wang, and S. Swaddiwudhipong, "Elastic buckling analysis of ring-stiffened cylindrical shells under general pressure loading via the Ritz method," *Thin-walled Struct.*, vol. 35, no. 1, pp. 1–24, 1999.

[18] V. L. Krasovsky and V. V Kostyrko, "Experimental studying of buckling of stringer cylindrical shells under axial compression," *Thin-Walled Struct.*, vol. 45, no. 10–11, pp.

877–882, 2007.

[19] B. C. Cerik, H.-K. Shin, and S.-R. Cho, “Probabilistic ultimate strength analysis of submarine pressure hulls,” *Int. J. Nav. Archit. Ocean Eng.*, vol. 5, no. 1, pp. 101–115, 2013.

[20] B. C. Cerik and S.-R. Cho, “Numerical investigation on the ultimate strength of stiffened cylindrical shells considering residual stresses and shakedown,” *J. Mar. Sci. Technol.*, vol. 18, pp. 524–534, 2013.

[21] S.-R. Cho, Q. T. Do, and H. K. Shin, “Residual strength of damaged ring-stiffened cylinders subjected to external hydrostatic pressure,” *Mar. Struct.*, vol. 56, pp. 186–205, 2017.

[22] A. Zingoni, “Liquid-containment shells of revolution: A review of recent studies on strength, stability and dynamics,” *Thin-Walled Struct.*, vol. 87, pp. 102–114, 2015.

[23] P. Radha and K. Rajagopalan, “Ultimate strength of submarine pressure hulls with failure governed by inelastic buckling,” *Thin-walled Struct.*, vol. 44, no. 3, pp. 309–313, 2006.

[24] O. Temami, A. Ayoub, D. Hamadi, and I. Bennoui, “Effect of boundary conditions on the behavior of stiffened and un-stiffened cylindrical shells,” *Int. J. Steel Struct.*, vol. 19, no. 3, pp. 867–878, 2019.

[25] S. A. Elkholy, A. A. Elsayed, B. El-Ariss, and S. A. Sadek, “Optimal finite element modelling for modal analysis of liquid storage circular tanks,” *Int. J. Struct. Eng.*, vol. 5, no. 3, pp. 207–241, 2014.

[26] F. N. U. Tabish and I. H. P. Mamaghani, “Buckling Analysis of Cylindrical Steel Fuel

Storage Tanks under Static Forces”.

[27] Z. Li, H. Pasternak, and A. Jaeger-Canas, “Buckling of ring-stiffened cylindrical shell under axial compression: Experiment and numerical simulation,” *Thin-Walled Struct.*, vol. 164, p. 107888, 2021.

[28] S.-R. Cho, T. Muttaqie, Q. T. Do, S. Kim, S. M. Kim, and D.-H. Han, “Experimental investigations on the failure modes of ring-stiffened cylinders under external hydrostatic pressure,” *Int. J. Nav. Archit. Ocean Eng.*, vol. 10, no. 6, pp. 711–729, 2018.

[29] J. Y. Kim, “ANSYS workbench training manual,” *Taesung Softw. Eng.*, pp. 9–28, 2010.

[30] S. P. Timoshenko, “Einige stabilitätsprobleme der elastizitätstheorie,” *Zeitschrift für Math. und Phys.*, vol. 58, no. 4, pp. 337–385, 1910.

[31] L. Huei-Huang, “Finite Element Simulations with Ansys Workbench 2021.” SDC Publications: Ulaanbaatar, Mongolia, 2021.

[32] S. M. Fatemi, H. Showkati, and M. Maali, “Experiments on imperfect cylindrical shells under uniform external pressure,” *Thin-Walled Struct.*, vol. 65, pp. 14–25, 2013.

[33] J.-G. Teng and J. M. Rotter, *Buckling of thin metal shells*. CRC Press, 2006.

[34] A. Raza and M. S. Jameel, “Investigation of flexural behavior of reinforced concrete beams using 3D finite element analysis,” *J. Numer. Methods Civ. Eng.*, vol. 7, no. 1, pp. 37–56, 2022.

[35] N. Yamaki, *Elastic stability of circular cylindrical shells*. Elsevier, 1984.

[36] E. N. 1993-1-6, “Eurocode 3: Design of steel structures–part 1-6: Strength and stability of shell structures.” CEN Brussels, 2007.

[37] S. B. Batdorf, “A simplified method of elastic-stability analysis for thin cylindrical shells,” 1947.

[38] J. H. S. Almeida Jr, M. L. P. Tonatto, M. L. Ribeiro, V. Tita, and S. C. Amico, “Buckling and post-buckling of filament wound composite tubes under axial compression: Linear, nonlinear, damage and experimental analyses,” *Compos. Part B Eng.*, vol. 149, pp. 227–239, 2018.

[39] R. V. Southwell, “On the analysis of experimental observations in problems of elastic stability,” *Proc. R. Soc. London. Ser. A, Contain. Pap. a Math. Phys. Character*, vol. 135, no. 828, pp. 601–616, 1932.

[40] J. Roorda, “Some thoughts on the Southwell plot,” *J. Eng. Mech. Div.*, vol. 93, no. 6, pp. 37–48, 1967.

[41] W. HORTON and F. CUNDARI, “On the applicability of the Southwell plot to the interpretation of test data from instability studies of shell bodies,” in *8th Structural Dynamics and Materials Conference*, 1969, p. 1167.

[42] S. S. Seleim, “INTERACTIVE BUCKLING OF RING-STIFFENED CYLINDERS SUBJECTED TO LATERAL PRESSURE.,” 1985.

[43] K.-J. Bathe, *Finite element procedures*. Klaus-Jurgen Bathe, 2006.

[44] H. Ullah, “Buckling of thin-walled cylindrical shells under axial compression,” *Int. J. Numer. Methods Eng.*, vol. 79, no. 11, pp. 1332–1353, 2009.

[45] Z. U. R. Tahir, *Buckling of thin cylindrical shells under axial compression*. The University of Manchester (United Kingdom), 2016.